MONTORING CRACKING OF A SMECTITIC VERTISOL USING THREE-DIMENSIONAL ELECTRICAL RESISTIVITY TOMOGRAPHY

A Thesis

by

JASON PAUL ACKERSON

Submitted to the Office of Graduate and Professional Studies of
Texas A&M University
in partial fulfillment of the requirements for the degree of

MASTER OF SCIENCE

Chair of Committee,	Kevin J. McInnes
Committee Members,	Cristine L.S. Morgan
	Mark E. Everett
Head of Department,	David Baltensperger

December 2013

Major Subject: Soil Science

ABSTRACT

Upon desiccation, the matrix of Vertisols and other expansive soils shrinks. Matrix shrinkage results in the formation of cracks that can alter the hydrology of the soil. Despite the importance of cracks, many hydrologic models do not account for cracking due in part to a lack of reliable information on the development and morphology of cracks. Electrical resistivity tomography (ERT) has shown promise as a new, non-destructive method of monitoring cracking in the field. We investigated the use and limitation of ERT for monitoring the spatial degree and extent of cracking in a Texas Vertisol. First, we examined the relationship between soil water content and ERT derived bulk soil electrical resistivity. Results showed that when the soil was cracked, ERT is insensitive to changes in water content with the electrical resistivity of the soil much greater than would be predicted from changes in water content alone. For a direct measurement of the degree and extent of cracking, we filled cracks with cement, excavated the soil, and photographed the exposed cracks. Comparing direct crack measurements with ERT images of the electrical resistivity of the subsoil, we found that a simple linear model could describe the relationship between crack volume and bulk electrical resistivity. Unfortunately, the fit of this model was poor (R^2 from 0.4-0.6) and it showed little promise for accurately estimating crack volume. As a tool for monitoring cracks, it appears that ERT is best suited for identifying probable locations of cracks rather than quantitative evaluation of crack morphology.

DEDICATION

To Mary and Skip.

I wouldn't be here without you.

ACKNOWLEDGEMENTS

I am deeply indebted to my committee, Dr. McInnes, Dr. Morgan, and Dr. Everett. Their support and guidance helped me grow as a scientist and researcher. I would also like to thank my colleagues and fellow students from the Hydropedology research group. Whether they helped carry equipment, grind soil, or run lab analyses, they were an indispensable part of this project. Their hard work and dedication inspired me to work harder and to become a better scientist. I owe a particularly high level of gratitude to Haly Neely and Jose Fuentes. Thank you both for your patience. Finally, I must acknowledge the love and support of my family. They fostered a love of science that has proven to be an incredible gift. I would also like to thank my girlfriend Jill who keeps snacks in her purse in case I get hungry. The material in this thesis is based upon work supported by the Texas A&M AgriLife Research, a Cooperative Agreement with the USDA-NRCS Texas Soil Survey, and the National Science Foundation under Grant No. EAR 0911317.

TABLE OF CONTENTS

Page

LIST OF FIGURES

Page

LIST OF TABLES

Page

CHAPTER I

INTRODUCTION AND LITERATURE REVIEW

Vertisols, and other soils with high clay content, exhibit changes in volume due to changes in water content. As these soils absorb water, they swell, and as they desiccate, they shrink. The potential decrease in volume of a given mass of soil on drying can be as much as 40 percent from the fully hydrated state. As a consequence of shrinkage, surface and subsurface cracks form. Soil cracks can greatly alter the response of soil to rainfall and therefore are important features to consider in surface hydrology. Cracks in the soil facilitate the interception, channelization, and storage of stormwater that might runoff in the absence of surface cracks (Bouma, 1981; Arnold et al., 2005). Cracking also exposes subsoil surfaces to direct evaporative loss of water to the atmosphere (Ritchie and Adams, 1974). The effects of cracking on runoff, evaporation, and distribution of water in the soil profile are influenced by the magnitude, spatial distribution, and depth of cracking. Large cracks store more runoff and expose deeper sections of soil to evaporation and redistribution than small, shallow cracks. Cracks with openings located on topographic high-spots receive less runoff than those on low-spots.

Ignoring soil cracking in surface hydrology models can lead to large uncertainty in partitioning of rainfall (Arnold et al. 2005), but before cracking subroutines in hydrology models can be improved, the spatial and temporal cracking phenomena must be better understood. For example, knowledge how areal density, spatial distribution, depth, and volume of cracks change with water content across landscapes would be

useful in developing models to address their hydrologic impact. Development of such understanding has been slow, in part, due to a lack of accurate methods for measuring the size and spatial extent of cracks. One of the primary challenges in studying soil cracks is that cracks are difficult and time consuming to characterize. Development of novel techniques for rapid and accurate characterization of soil cracks would be beneficial.

One possible method of measuring soil cracks is through the use of electrical resistivity tomography (ERT). ERT uses measurements of electrical signals to develop an image of the subsurface electrical properties of a soil. Electrical properties of soils are influenced by the contrast of electrical properties of soil solids, water, and air. ERT has been used in soil science to measure water content (Daily et al., 1992; Zhou et al., 2001; Michot et al., 2003; Amidu and Dunbar, 2007, Rings et al., 2008; Schwartz et al., 2008; Amato et al., 2009; Srayeddin and Doussan, 2009; Brunet et al., 2010), coarse fragment content (Rey et al., 2006; Tetagan et al. 2012), and infiltration and water movement (French and Binely, 2004; Cassiani et al., 2009). ERT has also been used to measure soil cracking of repacked soil in the lab (Samouëlian et al., 2003, 2004; Sentenac and Zielinski, 2009; Greve et al., 2010b) and in the field (Greve et al., 2010a). It has yet to be shown that ERT can be used to measure areal density, depth, volume, and location of cracks under field condition and at scales of 5 to 10 m.

Measuring Soil Cracks

Crack Volume

Several approaches have been used to measure or estimate crack volume including measuring the amount of sand or wax required to fill cracks (Dasog and Shashidhara, 1993; Peng et al., 2006), physical measurements of depth, width, and length (Dasog and Shashidhara, 1993; Ringrose-Voase and Sanidad, 1996, Kishné, et al., 2009), or measurements soil subsidence and an assumption about the dimensionality of shrinkage (Bronswijk, 1989; Arnold et al., 2005, Dinka et al. 2013). Infilling of soil cracks allows for good accuracy and resolution of crack volume. A major drawback of infilling arises from the inability to use the method to track the temporal development of a crack. Once a crack has been filled, the infill alters future changes in the crack. Additionally, due to practical limitations, infilling is only viable for studying small areas.

Crack volume can also be estimated from measurements of crack width at the surface and crack depth. Direct measurements of width and depth have been made along transects (El Abedine and Robinson, 1971; Ringrose-Voase and Sanidad, 1996) and within fixed plots (Sharma and Verma, 1977; Dasog and Shashidhara, 1993; Yassoglou et al., 1994; Kishné et al., 2009). Crack volume is calculated by multiplying crack depth, width, and length with a scalar based on an assumed crack cross-sectional geometry of cracks. Geometry scalars have ranged from one, for straight-sided cracks (Dasog and Shashidhara, 1993; Yassoglou et al., 1994), to one-third, for isosceles-triangle-shaped cracks (El Abedine and Robinson, 1971; Ringrose-Voase and Sanidad, 1996). Dasog and Shashidhara (1993) found good agreement between calculated

volumes and those measured by infilling. This method is limited by its tedious, time-consuming nature and the inaccuracy of crack width measurements in Vertisols that self-mulch, where crumbly surface structure results in ill-defined crack edges.

The most common method of estimating crack volume is through measurements of vertical movements of the soil surface and subsoil. Vertical soil movement is measured by placing anchors in the soil at various depths. To measure soil shrinkage and swelling, the changes in heights of rods attached to the anchors are monitored electronically using linear-displacement sensors (Coquet, 1998) or by manually with a survey level (Bronswijk, 1989; Cheng and Pattry, 1993; Arnold et al., 2005; and Kirby et al., 2003, Dinka et al. 2013). By assuming that the soil shrinks equidimensionally, crack volume can be calculated using the following equation (Bronswijk, 1989):

$$V_{crack} = \left[1 - \left(1 - {}^{\Delta z}/_{z}\right)^{3}\right] z^{3} \qquad [1]$$

where V_{crack} is crack volume in m^3, z and Δz are the initial layer thickness and layer shrinkage in m, respectively.

One of the challenges with this technique is in monitoring changes along a single vertical line through a soil profile. Horizontal distribution of anchors introduces problems with spatial variability that is not easily addressed. In addition, the accuracy of estimates of crack volume from vertical shrinkage relies on the assumption that the dimensionality of the shrinkage can be defined. Although Bovin (2007), demonstrated that, in the lab, soil cores shrank equidimensionally, equidimensional shrinkage of soil in the field remains unverified.

Another assumption made in subsidence-based methods is that soil collapses on itself as it shrinks. Dinka et al. (2013) found that, given observed changes in soil water content, measured soil subsidence was lower than would be predicted by using the equations of Bornswijk (1991). The authors suggested that as the soil shrank it did not collapse vertically, leading to the observed discrepancy. Additionally, as it shrinks, individual soil units can settle along slippage faces or slickensides, which are oriented roughly 45 degrees to the surface. As a soil unit settles along a slickenside, it may fill in crack volume that opened through vertical shrinkage biasing subsidence measurements. To our knowledge, no study has verified that estimates of crack volume from shrink-swell measurements agree with those found using independent measurements of crack volume.

Crack volume can be expressed using several units predominantly m of m^3. In this study we will express crack volume as the porosity generated by cracks, using units of m^3m^{-3}. Crack porosity is a subset of the total soil porosity and is defined as the volume of cracks per volume of soil.

Crack Density

Along with volume, crack density is a key factor in Vertisol hydrology. The greater the density of cracks, the greater the capacity to capture rainfall. Crack density has been defined in three ways: as a horizontal length, horizontal area, or vertical volume per unit area of soil surface. Horizontal length and area can be measured directly from surface cracks: however, volume must be calculated using assumed crack geometry and measured crack depths if measurements are to be made nondestructively.

Length has been estimated from hand measurements (El Abedine and Robinson, 1971; Dasog and Shashidhara, 1993; Ringrose-Voase and Sanidad, 1996) and photographs (Vogel et al., 1993, 2005; and Lakshmikantha et al., 2009). Area has been estimated from hand measurements in the field (Yassoglou et al., 1994; Kishné et al., 2009) and from photographs in the lab (Moureau et al., 1999; Peng et al., 2006) and in the field (Waller and Wallender, 1993; Velde, 1999, 2001; Baer et al., 2009).

One of the drawbacks of estimating crack density from direct measurements, as discussed earlier, is that hand measurements are time-consuming and are only feasibly on small scales without a considerable investment in labor. Photographic methods offer a viable alternative. Many photographs can be taken of the same soil in a short period of time allowing larger areas to be monitored with higher temporal resolution. However, photographs have limitations. Vegetation can block view of the soil surface and interfere with analysis, and therefore the soil must be bare or the vegetation trimmed close to the surface during measurement (Baer et al., 2009). The disadvantage of trimming the vegetation close to the surface is that the vegetation influences evaporation and the rate of crack development (Sharma and Verma, 1977); measurements made on bare or cultivated soil may not be representative of those made on vegetated soils. Additionally, photographs provide no depth data and therefore limit accurate estimation of crack volume density.

Spatial Patterns and Variability of Cracking

Crack orientation can play a critical role in the influence that cracks have on field-scale hydrology. Cracks oriented parallel to the contour lines of the slopes will

more likely intercept runoff than those running down the slope. Crack orientation patterns and size distributions are dependent on soil type (Yassoglou et al., 1994; Velde, 1999), vegetation cover (Sharma and Verma, 1977; Dasog and Shashidhara, 1993; Baer et al., 2009), irrigation and cultivation practices (Waller and Wallender, 1993; Cheng and Pettry, 1993), and microtopographies (Kishné et al., 2009). These factors vary at field and landscape scales contributing to spatial variability in cracking. As noted by Kishné et al. 2009, the spatial and temporal trends of cracking are best investigated by large continuous plots. Large-scale studies are necessary for understanding crack variability yet are lacking in the literature. Most studies have been conducted on plots smaller than 10 m^2.

Electrical Resistivity Tomography

Electrical resistivity tomography is a noninvasive near-surface geophysical technique that maps the electrical properties of the subsurface and can be applied to scales ranging from centimeters to tens of meters. It has been used successfully in the fields of archeology, hydrogeology, geotechnical engineering, geology, environmental remediation, and soil science (Pellerin, 2002). Electrical resistivity is defined as the ability of a medium to impede the flow of electrical current. Resistivity is commonly expressed in units of Ωm (m S^{-1}) and is the reciprocal of electrical conductivity (commonly expressed in S m^{-1} or mho m^{-1}). Typical values of resistivity range from 10^5 Ωm for crystalline igneous rocks to 100 Ωm for unconsolidated clay (Robinson and Coruh, 1988). At the voltages used in ERT, electrical charge cannot pass through air, thus the resistivity voids or cracks can be considered infinite. The high resistivity

contrast between clay (100 Ωm) and air-filled cracks (infinite resistivity) makes ERT sensitive to cracking.

Electrical resistivity of soil is influenced by many properties including soil texture, water content, porosity, tortuosity, solute concentration, and temperature (Samouëlian et al., 2005). An empirical relationship between water content and resistivity of sandstone (Archie, 1942), known as Archie's law, defines the relationship between total resistivity, pore-water resistivity, and porosity:

$$\rho/\rho_w = a^{-m} \quad [2]$$

where ρ and ρ_w are the total resistivity and pore-water resistivity, respectively, and is the porosity. Archie's law also contains two fitting parameters specific to the medium; Archie's constant *a*, and Archie's cementation exponent *m*. Archie's constant and cementation exponent are dependent on pore geometry (Robinson and Coruh, 1988). Due to the empirical nature of Archie's law and the complexities of pore geometry, mechanistic descriptions of these parameters remains poorly understood (Glover et al., 2000).

Archie's law was developed on saturated sandstones but can be reformulated to account for variable degrees of saturation (Waxman and Smits, 1968):

$$S^n = a\rho_w\phi^{-m}\rho^{-1} \quad [3]$$

where *S* is saturation percentage and *n* is an additional fitting parameter. The parameter *n* is commonly assumed to equal two (Robinson and Coruh, 1988). This modification has been shown to be successful for a large range of soils except for those with high clay contents (Frohlich and Park, 1989).

In clay soils, Archie's law is inaccurate because it does not account for the movement of charges along the surfaces of soil particles nor for the consolidation of clay particles on drying. Rhoades et al. (1976) reformulated Archie's law to account for the conductivity of soil surfaces:

$$1/\rho = 1/\rho_w\,(a\theta^2 + b\theta) + 1/\rho_s \qquad [4]$$

where ρ represents the total soil resistivity, ρ_s represents resistivity of soil particle surface, θ represent volumetric water content of the soil, and a and b are fitting parameters. By accounting for conduction of current within the solid phase of the soil Rhoades et al. (1976) demonstrated that electrical resistivity could be used to predict soil water content in high clay soils.

Measurement of Soil Resistivity

Application of electrical resistivity tomography to soils in the field is a two-step process, field measurements followed by inversion of the signal using a computer inversion algorithm. To make a field measurements, electrodes are inserted into the soil surface in the form of an array. Current is applied to two transmission electrodes and an electrical potential is measured between two separate, remote, receiver electrodes (Fig. 1). Using the electrode geometry, the apparent resistivity of the volume of surrounding soil can be calculated. By increasing separation distance between electrodes, signals travel through larger soil volumes and arrays integrate resistivity from a larger volume of soil allowing for imaging deeper into the soil. Modern resistivity surveys are taken using automatic survey equipment. This automatic equipment uses a computer controlled switching unit to rapidly select between different electrode configurations and

spacings. By making many measurements with different array configuration and spacing, a single survey can rapidly generate many data points.

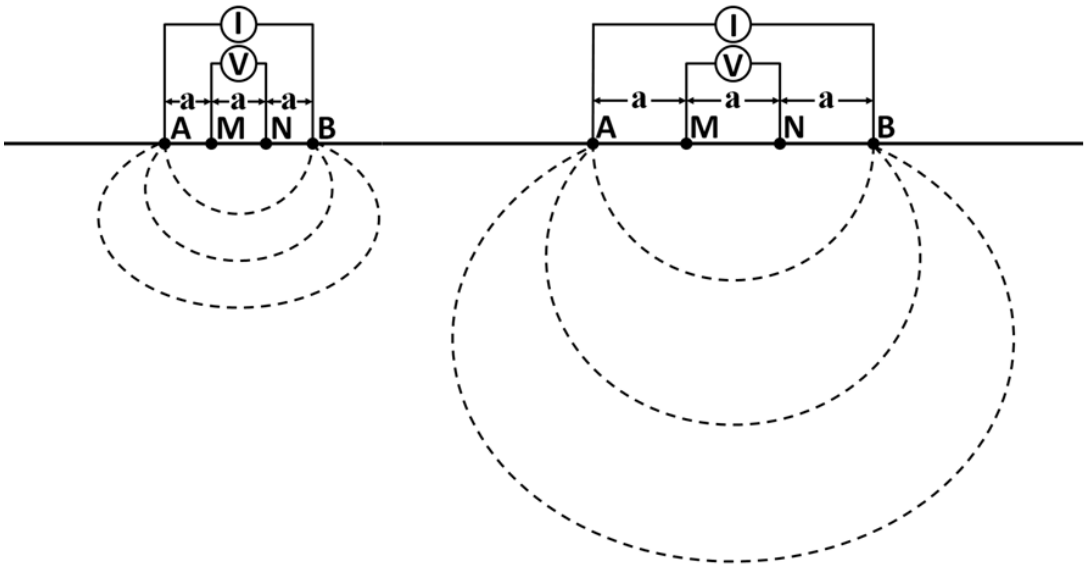

Figure 1. Soil resistivity measurement using a Wenner array. Current (I) is generated between electrodes A and B and voltage (V) is measured at electrodes M and N. As electrode separation (a) increases, signals travel through a deeper and larger volume of soil.

After field measurements are taken, resistivity maps are generated using a computer algorithm known as an inversion. Inversion is the final step in electrical resistivity tomography and generates two or three-dimensional resistivity maps of the subsurface from surface measurements (Oldenburg, 1990). To achieve the maps, the inversion algorithm performs a search that attempts to find the resistivity map that best fits a given set of field resistivity measurements. At the start of inversion, the algorithm generates

an initial map of subsurface resistivity structure. This map is a representation of the resistivities of individual layers or blocks within a finite element solution for electrical current flow in the soil (Samouëlian et al., 2005)

Once an initial map is generated, the algorithm performs a forward calculation. In the forward calculation, the algorithm simulates a resistivity measurement on the initial finite element map generating a set a synthetic resistivity measurement for each real measurement from the real field data. Next, in the search step, the algorithm calculates the value of an objective function from simulated and real field data. The objective function commonly incorporates some metric to quantify model roughness or complexity and misfit between simulated and real data (Pellerian, 2002). The goal of an inversion is to minimize the value generated by the objective function (Nobes 1996). To do this, the algorithm modifies electrical properties of the finite elements. With the updated map, a new forward calculation and assessment of the value of the objective function are performed. The cycle of parameter modification and forward calculation steps is repeated until the value generated by the objective function is minimized to a desired level resulting in the final resistivity map.

Crack Monitoring with Electrical Resistivity Tomography

Despite its challenges ERT has emerged as useful tool in soil science. Resistivity is influenced by many factors including water content, solute concentration, and soil texture. Soil scientists have taken advantage of these sensitivities and used resistivity to measure soil water content, groundwater levels, soil heterogeneity, and infiltration (Samouëlianet al., 2005). Soil cracks when filled with air, as is the case under most field

conditions, increase the bulk soil resistivity. This has been demonstrated in the laboratory by Samouëlian et al. (2003) who found that readings from small, centimeter-scale, two-dimension resistivity arrays were sensitive to soil cracks. Sentenac and Zielinski (2009) used a similar survey setup to monitor cracking in a drying clay paste under laboratory conditions. They found that inverted ERT images could identify crack depth and location. Both these studies demonstrated the feasibility of ERT for monitoring cracking under controlled laboratory conditions.

Field-scale ERT measurements have been made in cracking soil by Amidu and Dunbar (2007). As part of their study, two-dimensional ERT surveys were made on a Vertisol in central Texas in an attempt to measure the spatial distribution of soil water content. Their results demonstrated that measurements made during dry periods were highly influenced by surface cracking, leading to inaccuracies in soil water content estimations.

One of the primary challenges in using two-dimensional ERT to measure soil cracks is that cracked soil is anisotropic, meaning that apparent resistivity measurements are dependent on the angle of resistivity survey relative to crack orientation. ERT will only detect a crack if the crack is oriented roughly perpendicular to the survey line (Samouëlian et al., 2003). To mitigate anisotropy effects, Samouëlian et al., (2004) recommended using 3D surveys; however, such surveys have yet to be conducted in Vertisols under field conditions. By measuring the degree of anisotropy, some researchers have been able to detect cracks in the lab (Samouëlian et al., 2004) and in the field (Greve et al., 2010a/b). Field measurements required installation of subsurface

electrodes and were limited to a single small (0.5-m square) plot. These small-scale tests, while valuable, provide limited information on the spatial patterns of cracking which is needed to understand and predict cracking at large scales.

Another challenge for using resistivity to measure soil cracks is that ERT is sensitive to water content as well as cracking. To isolate the effects of cracking on resistivity, the effects of water-content on soil matrix resistivity (resistivity of soil between cracks) may need to be accounted for and corrected. To describe the relationship between soil water content and resistivity, it is common to develop an empirical function similar to the one suggested by Rhoades et al. (1976). These functions can be parameterized for an individual soil in the lab with repacked soil (Amidu and Dunbar 2007; Brunet et al., 2010), on intact cores (Rhoades et al. 1976), or in the field using independent measurements of soil water content and resistivity (Michot et al., 2003; Schwartz et al., 2008; Srayeddin and Doussan, 2009). Only calibrations made on intact soil cores, where structure is preserved, can account for the effects of aggregates on bulk soil resistivity (Rhoades et al., 1976) and is particularly important in Vertisols where the expression of structure is water content dependent. Once an empirical relationship is established, water content, measured independently from ERT can be used to predict and correct for changes in soil matrix resistivity.

Study Scope

Electrical resistivity tomography shows promise as a technique for measuring soil cracks. As a noninvasive technique, it allows the same area to be surveyed multiple times, providing the opportunity for measuring soil cracking with a desirable temporal

resolution. ERT has the benefit of functioning at scales on the order of tens of square meters, providing larger spatial coverage compared to current methods. However, before ERT can be used to monitor cracking in the field, several questions need to be addressed:

1. In the field and at moderate scales, to what aspects of soil cracking is ERT sensitive? Specifically, can ERT be used to measure depth, areal density, location, and volume of cracks? If so, with what resolution?
2. To what degree do water content and cracking interact to influence ERT images of the subsurface? To accurately monitor cracks using ERT, do water content induced changes in soil matrix resistivity need to be taken into account?

To answer these questions, we made measurements of soil resistivity and water content, over the course of a wetting and drying cycle on a 25 m^2 plot in a Vertisol. As the soil dries and cracks open, total resistivity should be influenced to a greater extent by cracking. Data collected for a range of water contents and cracking, provided a series of ERT surveys influenced by varying degrees of cracking. When cracking had reached its maximum, we filled cracks with cement and then excavated in horizontal layers. Photographs of the excavated crack pattern provided direct measurements of areal density, location, and depth of cracks. These direct crack measurements of crack geometry were then be compared to ERT images of electrical resistivity to determine what attributes of cracks ERT could be used to estimate.

One of the primary challenges in monitoring resistivity and cracking is that both are influenced by soil water content. Loss of soil water through evapotranspiration causes soil shrinkage and results in cracking but also increases the resistivity of the soil matrix. Additionally, cracking also increases soil resistivity. The effect of the correlated relationships between cracking, soil resistivity, and soil water content on final ERT images is still unstudied. By monitoring cracking, soil resistivity, and soil water content concurrently, we were able provide insight into the interaction between water content, cracking, and ERT.

When compared to previous studies, this work was unique in several ways. Firstly, the only published study using ERT on Vertisols in the field and at scales greater than a meter, was conducted in two dimensions. Due to the anisotropic nature of cracked soil, two-dimensional surveys are insensitive to cracking parallel to survey directions. Three-dimensional measurements are less prone to bias than two-dimensional ones. For example, if in a two-dimensional survey, cracks running parallel to the survey line will not be observed; the survey imparts a directional bias. If cracking exhibits a preferred orientation, such a survey may over or under represent the extent of cracking based on its direction relative to the direction of cracking. By measuring resistivity in three dimensions, resistivity we were to provide electrical resistivity data that is more robust to crack anisotropy.

In addition to removing anisotropy induced bias, this study was the first to first to measure soil resistivity, water content, and cracking independently. This has several advantages over previous studies which did not measure soil water content. Concurrent

data on crack porosity, bulk soil electrical resistivity, and soil water content helped determine the role of water content in final ERT based crack measurements.

CHAPTER II

THE ROLE OF SOIL WATER CONTENT IN THREE-DIMENSIONAL ELECTRICAL RESISTIVITY TOMOGRAPHY OF A VERTISOL

Introduction

In Vertisols, changes in soil water content result in changes in soil volume as shrinkage occurs on drying and swelling occurs on wetting. This shrink-swell behavior results in the formation and closure of desiccation cracks (Bronswijk, 1989; Arnold et al., 2005; Dinka et al., 2013). Cracks can store precipitation, prevent runoff (Arnold et al., 2005), and enhance evaporation (Ritchie and Adams, 1974). By functioning as macropores, soil cracks allow water to infiltrate deeper into the soil profile than would be possible if water flow only occurred within the soil matrix (Mitchell and van Genuchten, 1993). To better understand how desiccation cracks affect field-scale hydrology, the spatial structure and heterogeneity of cracks within the field must be characterized. One technique that may be useful in characterizing spatial heterogeneity of cracks within a field is electrical resistivity tomography (ERT).

With ERT, a voltage difference is applied to the soil with a pair of electrodes placed at strategic locations. A current flows between the electrodes, generating an electric field in the soil. Voltages along this electric field are measured with an array of electrodes and used to generate a spatial image of the electrical resistivity within the soil. Cracks essential provide infinite resistance to flow of electric current and ERT has been used to map soil cracks in a laboratory setting (Samouëlian et al., 2003, 2004; Sentenac

and Zielinski, 2009; Greve et al., 2010b). Greve et al. (2010a) used ERT to develop vertical profiles of cracking in the field. These profiles measured the presence of cracking with depth, however, profiles had small, 0.5-m^2 areal footprints and had limited applicability to field scale processes. On a larger scale, Amidu and Dunbar (2007) attempted to use ERT to map soil moisture to a depth of 1.2 m across a transect of a field of Vertisol soil. Their results showed high electrical resistivity anomalies near the surface which they attributed to the effect of cracks.

It is well understood that the electrical resistivity of the soil matrix is a function of water content, with increasing electrical resistivity associated with decreasing water content (Waxman and Smits, 1968; Samouëlian et al., 2005). A major limitation of previous studies to map cracks with ERT was a lack of independent measurements of soil water content. The lack of water content measurements has made it difficult to separate changes in electrical resistivity due to cracking from those due to changes in water content.

The objective of this study was to observe the combined effects of water content and cracking on ERT in a Vertisol in situ. To separate the effects of soil water content and cracking, laboratory measurements of the relationship between electrical resistivity and water content were compared with field measurements of the relationship based on ERT-determined resistivities and neutron moisture meter-determined water contents.

Materials and Methods

Study Location

The study site is located in Brazos County Texas on a terrace of the Brazos River. The soil is a Burleson clay, a fine smectitic thermic, Udic Haplustert (Soil Survey Staff, 2012) and the site was fenced for pasture, but has been left ungrazed for several years prior to the study. Slope was less than 0.01 m m^{-1} and there was no visual evidence of surface microtopography in the form of gilgai. A 4.5 m by 5 m study plot was located (30° 37' 54.8'' N, 96° 28' 59.1'' W) at the site in an area with uniform vegetative cover and evidence of shrinkage and swelling in the forms of open cracks and scars from previous cracks.

Field Measurements of Soil Water Content

Water contents within the plot were measured using a neutron moisture meter (CPN 503 Hydroprobe, InstroTek Inc., Concord CA). To accommodate use of the neutron moisture meter, vertical access tubes were installed on a 2-m grid within the plot (Fig. 2a). The access tubes were installed in August 2011 when the soil was dry and at its seasonally greatest degree of shrinkage. When a large crack was present at an intersection of the grid, the location of the access tube was shifted by 0.5 m. To install the access tubes, a 31.4-mm diameter soil core was taken to a depth of 2.1 m using a hydraulically driven probe (Giddings Machine Company, Windsor, CO). Samples from these cores were retained for laboratory analyses. A 50.8-mm diameter auger was then used to enlarge the hole left by removal of the core. To complete installation, 50.8-mm OD Schedule 20 PVC tubes were pushed into the holes. PVC tubes were used in favor

of the more commonly used aluminum tubes to prevent electrical interference with the ERT surveys.

Additional neutron access tubes were installed outside the plot area to facilitate calibration of the meter. For calibration, ratios of counts of thermalized neutrons returned from the soil relative to those returned from the instrument standard were recorded with depth. Then four soil cores, 38.1 mm in diameter, were extracted from within 0.1 m of the tube and cut into 0.1-m long segments. Volumetric soil water contents of core segments were determined by mass loss on oven drying at 105 °C and the original volume of a core segment. To cover the range of observable soil moisture contents in the field, samples were taken when the soil was near field capacity and when the soil was seasonally dry. A linear equation relating water content to count ratio was then determined. During the course of the study, vertical profiles of the volumetric soil water content within the plot were determined using the calibration equation and measurements of count ratios determined at 0.2 m intervals from 0.2 m to 1.2 m.

The effect of large cracks on neutron moisture meter readings is poorly understood. Neutron moisture meter measurements are generally assumed to be influenced by soil water content within a spherical region surrounding the sensor. In soil that is not cracked, Chansyk and Naeth (1996) proposed

$$r = (1.4 + 10 \cdot \theta)^{-1} \quad [5]$$

where r (m) is the radius of the sphere of influence and θ is the volumetric soil water content in m^3m^{-3}. For practical reasons, large cracks were avoided during installation of access tubes and for soil sampling when the meter was calibrated. As a result, the

calibration may have slightly overestimated water content of the bulk soil volume that included large cracks (Fityus et al., 2011). While it may be possible to correct for the effects of large cracks, any such effort would require knowledge of the geometry of the cracks within the volume of soil to which the neutron moisture meter is sensitive. Such information would be difficult to obtain without destructive sampling that would preclude future measurements of water content at the specific location.

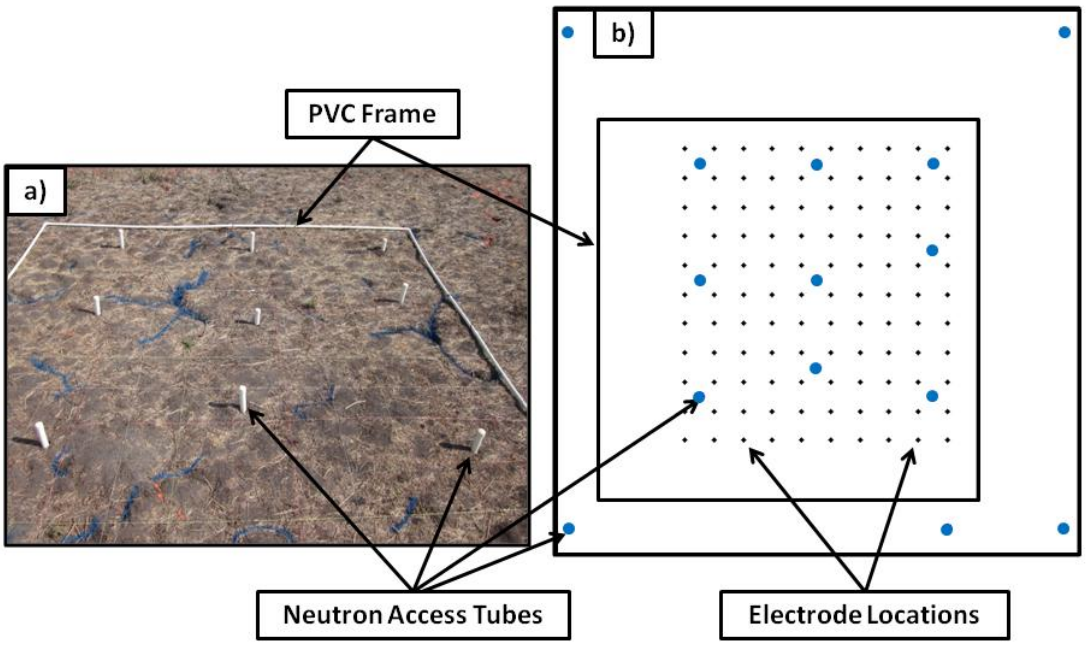

Figure 2. Photograph (a) and schematic (b) of the study plot showing the reference grid and neutron access tubes.

Electrical Resistivity Tomography

ERT surveys of the soil in the study plot were conducted on twelve dates from March to October 2012. On five of the dates (April through May 2012), cracks were not visible at the soil surface. On the remaining seven dates (August through mid-October 2012), surface cracks were visible. While it is possible that cracks existed in the subsoil without being visible at the surface, soil on dates without visible surface cracks will be referred to as non-cracked soil, and soil on dates with visible cracks will be referred to as cracked soil. The surveys were conducted using an AGI Supersting R8 resistivity/IP meter (Advanced Geosciences Inc., Austin TX). Electrodes consisting of 9.5-mm diameter stainless steel rods were positioned in a 10 by 11 grid with a 0.5-m spacing (Fig. 2b). At the beginning of each survey, electrodes were installed to a depth of 0.1 m. Electrodes were removed after completion of each survey. To insure that electrodes were positioned in the same location for each survey, a rigid rectangular frame of PVC pipe was constructed. Strings were mounted at 0.5-m spacing between parallel sides of the frame. The frame was left in place between measurements. When electrodes were installed, they were driven into the soil at the intersection of the strings.

Prior to collection of ERT data, contact resistances between the electrodes and soil were measured. High contact resistance can contribute to experimental errors propagated in ERT (Zhou and Dahlin, 2003). If the contact resistance exceeded 250 Ω, the soil surrounding the electrode was moistened by adding water until contact resistance fell below 250 Ω. The level of 250 Ω represented a compromise between reduction of contact resistance and application of water that could drain and directly influence

resistivity of the subsoil. When the soil was in a non-cracked state, contact resistance rarely exceeded 250 Ω. Soil temperature was measured at 0.1-m depth at the beginning of each survey to make a rough correction for the seasonal effect of temperature on resistivity.

Data for ERT were collected using a two-dimensional dipole-dipole array on the soil surface. This configuration allows for a three-dimensional survey. A three-dimensional survey was used to prevent bias due to the orientation of survey arrays relative to cracks. The effect of crack orientation on electrical resistivity data can be clearly observed in the case of a two-dimensional survey, where electrical resistivity data are collected along a single transect. In such a case, when the survey transect is oriented parallel to the crack, current can flow relatively undisrupted. If the survey transect is oriented perpendicular to the crack, current must flow underneath or around the crack, increasing the apparent electrical resistivity (Samouëlian et al., 2003).

The voltages measured at the surface and the known current applied to the soil were used to infer a three-dimensional image of subsurface electrical resistivity. The process of developing a subsurface image of electrical resistivity from surface measurements of voltage and applied current is called an inversion. During inversion, a computer algorithm is used to optimize a spatial set of apparent subsurface electrical resistivities to generate a match to data from surface measurements. In the inversion we used (EarthImager3D, AGI, Austin, TX), the set consists of electrical resistivities of elements in a finite element mesh representing the three dimensional soil domain where electrical current is likely to flow. The data to fit through inversion were the applied

current and voltages measured at the soil surface. The finite elements in the discretized space domain (grid) were comprised of rectangular-faced elements. The horizontal faces of each element were 0.125-m wide squares. In the surface layer, elements were 0.125-m tall. To save computational time and account for decreasing sensitivity of ERT with depth, in each successive layer, element height increased by a factor of 10%. Coarser elements could not achieve misfits below 10% for cracked soil.

EarthImager3D performs an Occam's style inversion (Advanced Geosicences, 2008). Occam's style inversion attempts to find a balance between the fit of the surface voltages and the complexity of the subsurface resistivity map. Complexity in the subsurface resistivity map is undesirable because often complexity results from measurement noise rather than complexity in the true electrical resistivity structure of the material (Constable et al., 1987; Samouëlian et al., 2005). The inversion algorithm is based on the work of Constable et al. (1987) who defined a forward function as:

$$\boldsymbol{d_m} = \boldsymbol{F}[\boldsymbol{m}] \qquad [6]$$

where $\boldsymbol{d_m}$ is the modeled synthetic data vector of length M, resulting from applying the forward function $\boldsymbol{F}$ to the model parameter vector $\boldsymbol{m}$ of length N. The term "synthetic" is used to describe $\boldsymbol{d_m}$ because it is not an actual measurement of soil electrical resistivity. The vector $\boldsymbol{d_m}$ may best be understood as the electrical resistivity that would be measured on a fictitious soil with an electrical resistivity described by the model vector $\boldsymbol{m}$. The value M is the number of data points collected from the field survey and N is the number of elements in the electrical resistivity model. The forward function in

EarthImager3D is based on Dey and Morrison (1979). For a given $\boldsymbol{d_m}$ and actual field measured data $\boldsymbol{d}$ a model misfit X^2 can be defined as:

$$X^2 = \|\boldsymbol{Wd} - \boldsymbol{Wd_m}\|^2 = \|\boldsymbol{Wd} - \boldsymbol{WF}[\boldsymbol{m}]\|^2 \quad [7]$$

where $\boldsymbol{W}$ is the M by M diagonal matrix for data weighting

$$\boldsymbol{W} = diag\{1/\sigma_1, , 1/\sigma_2, \ldots, 1/\sigma_M\} \quad [8]$$

and σ_j is the error associated with measurement d_j. Due to the ill posed nature of **F**, unconstrained minimization of X^2 can lead to "over fitting" the data where the final model is conforming to measurement noise rather than the general spatial trends in electrical resistivity of the soil, resulting in artifacts in the subsurface resistivity images (Constable et al., 1987; Zhang et al., 1995). To prevent over fitting, and thus avoid artifacts, misfit minimization is constrained by the addition of a model roughness term R:

$$R = \|\boldsymbol{\delta m}\|^2 \quad [9]$$

where δ is the N by N difference matrix describing the electrical resistivity difference between adjacent model elements. By weighting differences between vertical and horizontal elements separately, the difference matrix provides anisotropy constraints for the inversion. Anisotropy constraints are used to highlight or dampen vertical contrasts in inverted images. For the inversions preformed in this study, anisotropy constrains were chosen to highlight contrasts between horizontally adjacent elements in ERT images. Such constraints were necessary to achieve adequate fit to data measured on cracked soils.

The final inversion problem is a minimization of an objective function Φ consisting of a linear combination of data misfit X^2 and model roughness R

$$= X^2 + \lambda R \qquad [10]$$

where λ is the regularization strength. Regularization strength is defined by the user and functions to control the effects of tradeoff between X^2 and R. Higher regularization strength prevents over-fitting in inversion and leads to spatially smoother resistivity images, with smaller contrast between electrical resistivity of adjacent elements in the finite element mesh. Due to the expected high contrast in electrical resistivity for cracked soil, low regularization strength was used to prevent inversions from smoothing out anomalies that may have resulted from cracking.

If the forward function is linear, Φ can be minimized using Lagrange substitution. For electrical resistivity, the forward function is nonlinear and so Φ is minimized in an iterative fashion by making small, incremental changes to $\boldsymbol{m}$ using a conjugate gradient algorithm (Zhang et al., 1995).

The same regularization strength and anisotropy constraints were used for all inversions. In EarthImager3D, regularization strength is controlled by a smoothness factor and anisotropy constraints are controlled by the horizontal/vertical roughness ratio. The smoothness factor was set to 10 which was recommended for slightly rough models. The horizontal/vertical roughness ratio was set to 5 which represents the upper limit of recommended values, but was needed to achieve satisfactory RMS fits for cracked soils. Inversion was stopped if an RMS of 5% was achieved or RMS reduction from the previous iteration was less than 5% of the previous RMS. Convergence was

achieved faster for data collected when the soil was not cracked and generally resulted in lower RMS (Table 1).

Table 1. Convergence data for inversion of field data for non-cracked and cracked soil.

Non-cracked soil			Cracked Soil		
Date	**RMS**	**Iterations**	**Date**	**RMS**	**Iterations**
----------	--%--	----------	----------	--%--	----------
23 March	2.9	4	8 August	5.3	11
20 April	4.7	3	16 August	8.2	11
27 April	8.0	5	24 August	6.6	11
4 May	2.5	4	31 August	8.4	10
27 May	2.9	4	5 September	9.2	11
			13 September	9.9	11
			10 October	8.6	12

For each ERT survey, soil temperature was measured at 0.1-m depth. These temperature values were then used to correct electrical resistivities from ERT to 25°C using the equation of Keller and Frischknecht (1966)

$$\rho_{25°C} = \rho_T[1 + 0.025(T - 25)] \quad [11]$$

where $\rho_{25°C}$ and ρ_T are the electrical resistivity at 25°C and temperature T (°C), respectively. These temperature corrections were only approximate as temperatures vary with depth over diel and annual cycles (Campbell and Norman, 1998). Over the study period, temperature measured at 0.1 m ranged from 21.8°C to 31.7°C. Although the temperature correction does not account for temperature variations with depth, it does correct for gross differences in temperature over the seasonal course of the study.

Interpretation of data was performed on electrical resistivity values from the final iteration of the inversion after correction to 25°C. This data consisted of a three-dimensional sets of electrical resistivities located at the centroids of each element in the finite element mesh in the model and were used to generate three-dimensional images using the natural neighbor algorithm in MATLAB (R2012b, MathWorks Inc., Natick, MA).

Laboratory Calibration

To separate the effects of water content from cracking on resistivities estimated from ERT, functional models relating electrical resistivity of the soil matrix to water content of the matrix were needed. To facilitate development of these models, four 53.8-mm diameter core samples were collected outside the border of the experimental plot when the soil water content was near field capacity. A clod consisting of a 0.15-m section of the core was removed from the central area of each soil horizon. Visually observable cleavage faces and slickensides were avoided to reduce the potential of cracks forming in the clods during drying. Due to the thinness of the A and AB horizons, these horizons were combined and one clod was taken from the combined horizon. After the clods were selected, they were placed in nylon hairnets and coated with liquid saran (Soil Survey Staff, 1996). To determine if chemical or physical differences between horizons existed, additional cores were taken and analyzed for particle size and inorganic carbon content using the pipette and pressure calcimeter methods (Gee and Bauder, 1986; Sherrod et al., 2002), respectively.

In the laboratory, small incisions were made in the saran coating to allow movement of water into and out of the clods. Clods were then submerged in distilled water for 48 hours and allowed to hydrate. Once hydrated, the volume of each clod was measured using Archimedes' principle. Clods were then suspended in air and allowed to slowly dry from evaporation through the slits in the saran coating until the change in core mass between subsequent measurements was negligible. The drying process took roughly six weeks. Periodically during the drying process, the masses and electrical resistivities of the clods were measured. Since use of Archimedes' principle required resealing clods with saran, the volume of the clod was not measured again until the end of the dry-down, and once more after being oven dried. To approximate volumetric water content of a shrinking clod, change in volume of the clod was modeled using the equation of Olsen and Haugen (1998)

$$e = 0.5\left[\lambda_3\vartheta + \lambda_2 + \sqrt{(\lambda_3\vartheta + \lambda_2)^2 - 4\lambda_2(1-\lambda_1)\vartheta}\right] \quad [12]$$

where e is the soil void defined as $e = V_p/V_s$ and ϑ is the soil moisture ratio defined as $\vartheta = V_w/V_s$. The terms V_p, V_s, and V_w represent the volume of soil pores, soil solids, and soil water, respectively. The terms λ_1, λ_2, and λ_3 are fitting parameters. By definition, $\lambda_3 = 1$ and $\lambda_2 = e(\vartheta=0)$. To approximate λ_2, $e(\vartheta=0)$ was estimated using clod volume measured at oven dry water content. The remaining parameter λ_1 was fixed at 0.045. This value was chosen because the physical properties of Burleson clay most closely matched the physical properties of soils with published values of λ_1=0.045 (Olsen and Haugen, 1998). From the void and moisture ratios, volumetric water content was then calculated using:

$$\theta = {\vartheta}/{(1 + e(\vartheta))} \quad [13]$$

One limitation Eq. 12 is that it does not account for shrinkage in the structural shrinkage phase. At high moisture ratios in highly structured soils, structural shrinkage may occur where water drains from large pores without an appreciable decrease in soil volume. By ignoring structural shrinkage, there was a chance that, at high water contents, Eq. 12 overestimated the amount of shrinkage, resulting in positively biased water contents. For clay soils at high water contents, electrical resistivity changes only slightly for a given change in soil water content (see later discussion), and any error in water content estimation in this range would have little influence on the final relationship between electrical resistivity and water content.

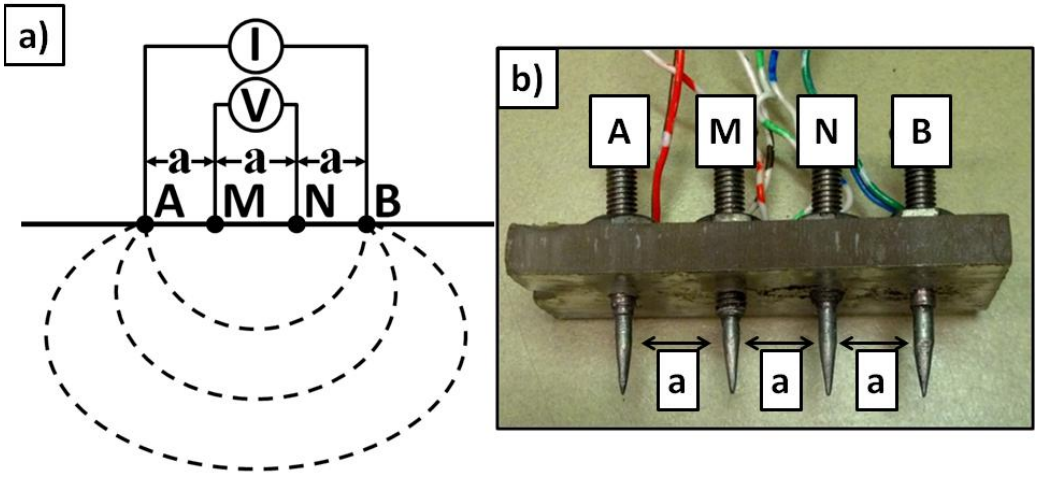

Figure 3. Schematic of the electrical field generated using a Wenner electrode array (a) and photograph of the electrode array used in laboratory measurement of electrical resistivity (b).

Electrical resistivities of the clods were measured using a four-pronged Wenner array (Fig. 3) and an analog resistance meter (Model 400A, M.C. Miller Co. Inc., Sebastian, FL). The array consisted of 2-mm diameter, conically pointed, stainless steel electrodes spaced 12.7-mm apart. Electrodes were affixed to a rigid acrylic sheet to maintain constant electrode geometry through the experiment. For each clod, five resistance measurements were made. Measurements were spaced roughly equally around the circumference of the clod to average-out variation in electrical resistivity within the clod. When possible, measurements were made in the same locations through the course of drying. For any given water content, the electrical resistivity of clods was assumed to be equal to the electrical resistivity of the soil matrix. Resistance values were then converted to electrical resistivity using:

$$\rho_{matrix} = 2\pi aR \qquad [14]$$

where ρ_{matrix} is calculated electrical resistivity (Ωm), a is electrode spacing (m), R is measured resistance (Ω). The accuracy of the resistance meter and laboratory array was checked by measuring the electrical resistivity of potassium chloride solutions of known resistivity. At the time of each electrical resistivity measurement, soil temperature was measured using a digital thermometer and matrix electrical resistivity was then corrected to 25 °C using Eq. 11.

Several equations have been used in soil science to relate soil electrical resistivity or its reciprocal, electrical conductivity, with water content. One such equation is a modified form of Archie's law (Archie, 1942) for unsaturated media developed by Waxman and Smits (1968):

$$\rho_{matrix} = (a\theta^n + b)^{-1} \; for \; \theta > \left(-b/a\right)^{1/n} \quad [15]$$

where ρ_{matrix} is the soil electrical resistivity, θ is the volumetric water content and a, b, and n are fitting parameters. The Waxman and Smits model (WS model) has been used for a large range of soils including sands (Rings et al., 2008) and silt loam (Garré et al. 2010; Garré et al. 2011). In clay soil, Amidu and Dunbar (2007) fit a slightly different model assigning electrical resistivity as the dependent variable:

$$\theta = c{\rho_{matrix}}^m + d \quad [16]$$

For all the models used in the study, values of the parameters were determined by Gauss-Newton nonlinear least squares and then analysis of covariance was used to compare differences in these parameters between horizons (R Core Team, 2013).

Results and Discussion

The soil at the study plot was fairly uniform with depth (Table 2). Soil texture for all horizons was clay with a slight increase in clay content deeper in the profile. Along with the small increase in clay content, there was a small increase in inorganic carbon content with depth. Inorganic carbon content was measured because it dilutes shrink-swell potential (Dinka et al., 2013), but the magnitude of and range in contents measured here were low enough to have minimal effect.

Table 2. Properties of Burleson Clay at the study plot.

Depth	Horizon	Munsell Color	Structure	Sand	Clay	Inorganic Carbon
----	----------	----------	----------	----------	----------	g kg^{-1} ------
0-14	A	2.5Y 2.5/1	Strong Granular	170	540	0.1
14-38	AB	2.5Y 2.5/1	Moderate Angular blocky	150	570	0.1
38-66	Bss1	2.5Y 2.5/1	Strong Wedge	160	570	0.4
66-	Bss2	2.5Y 2.5/1	Strong Wedge	160	580	1.3
101-	Bssk	2.5Y 3/1	Strong Wedge	130	600	2.8

Relationship Between Electrical Resistivity and Water Content

For the Burleson clay soil in this study, both the Waxman and Smits model (Eq. 15) and the Amidu and Dunbar Model (Eq. 16) were fit to laboratory measurements of clod electrical resistivity and water content. The Waxman and Smits model fit the data most poorly with an RMSE = 190 Ωm and R^2 = 0.63. The Amidu and Dunbar model fit the data better with an RMSE = 9.6 Ωm and R^2 = 0.76. To achieve a slightly better fit to the data, the following empirical model was used

$$\rho_{matrix} = e^{(\alpha\, \theta^{\gamma} + \beta)} \quad [17]$$

This model showed the best fit to laboratory data with an RMSE = 8.3 Ωm and R^2 = 0.84 with model parameters of 0.0087, -2.40, and 0.733 for α, γ, and β, respectively. Separate calibrations of Eq. 17 were performed for each soil horizon, but there was not a significant difference between model parameters for each horizon so a single model was fit to the combined data. All terms in the model were significant at the 0.001 probability level.

Both Houston Black clay, that Amidu and Dunbar (2007) investigated, and Burleson clay are classified as fine, smectitic, thermic Udic Haplusterts, and both exhibit similar mineralogy and clay content. Amidu and Dunbar used rewetted and packed soil that had been homogenized by grinding and mixing after being dried. Naturally aggregated soil, as was used here, could exhibit more complex and spatially variable electrical flow paths which could explain some of the slight differences between the data presented here and the model used by Amidu and Dunbar. Additionally, for the data collected in this study, there was a lack of data around 0.15 m^3m^{-3} water content (Fig. 4). This lack of data may have influenced the final fit of the laboratory model and contributed to deviation between the fitted model and the model used by Amidu and Dunbar.

In soils that do not shrink, pores desaturate as the soil dries. When pores desaturate, the electrical resistivity of those pores increases along with an increase in the tortuosity of the electrical path through the soil. The combined effect of increased resistivity and increasedtortuosity leads to increased electrical resistivity of the soil matrix (Lesch and Corwin, 2003). In a Vertisol, pores shrink with loss of water and can remain saturated over an appreciable range in water content as the soil dries. The greater the shrink-swell potential of a soil, the larger the range pores remain saturated. Because of the shrinkage of the inter-aggregate pores, increased matrix electrical resistivity due to de-saturation of inter-aggregate pores requires a greater total loss of soil water from shrink-swell soils compared to rigid soils. In addition, shrinkage may lead to increased

electrical current flow through particle-particle contact as bulk density increases (Seladji et al., 2010).

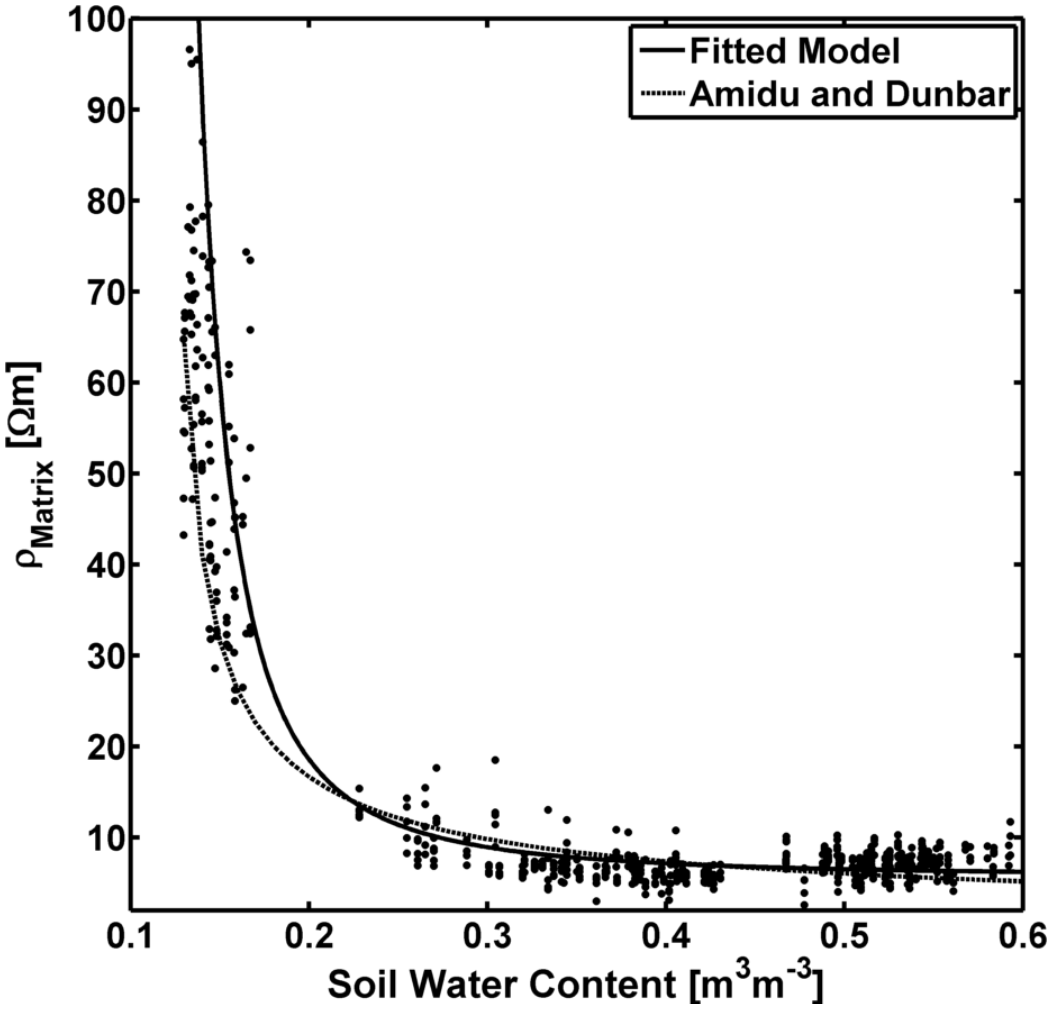

Figure 4. Electrical resistivity of Burleson clay as a function of water content (Eq.17). The relationship developed by Amidu and Dunbar (2007) for the Houston Black clay (Eq. 16).

The difference between shrink-swell and rigid soils is apparent when comparing the relationship between electrical resistivity and water content of soils with different texture. For a decrease in water content from 0.4 to 0.3 m^3m^{-3}, Rings et al. (2008) found a 40% increase in electrical resistivity for a sandy soil, and Garré et al. (2011) found a 37% increase for silt loam soil. For Burleson clay, the increase was only 8% (Fig. 4). While ERT has been used to measure soil water content (Michot et al., 2003; Schwartz et al., 2008; Srayeddin and Doussan, 2009; Garre et al. 2010), the low sensitivity to changes in soil water content can leave prediction of soil water in Vertisols (e.g., Burleson and Houston Black clays) highly susceptible to the effects of measurement errors in resistivity.

Electrical Resistivity of Cracked and Non-Cracked Soil

In general, electrical resistivities of the soil estimated from ERT were much greater in cracked soil compared to non-cracked soil. For example, mean electrical resistivity at 0.2-m depth was over 4 orders of magnitude greater in the cracked soil compared to the non-cracked soil (Fig. 5). In addition, when cracks were observed at the soil surface, electrical resistivity images had a much higher relative range in values and more fine-scale structure compared to images generated from data from non-cracked soil. These small features had very high electrical resistivity. For their two-dimensional ERT surveys, Amidu and Dunbar (2007) saw similar high-resistivity anomalies which they suggested were caused by cracks.

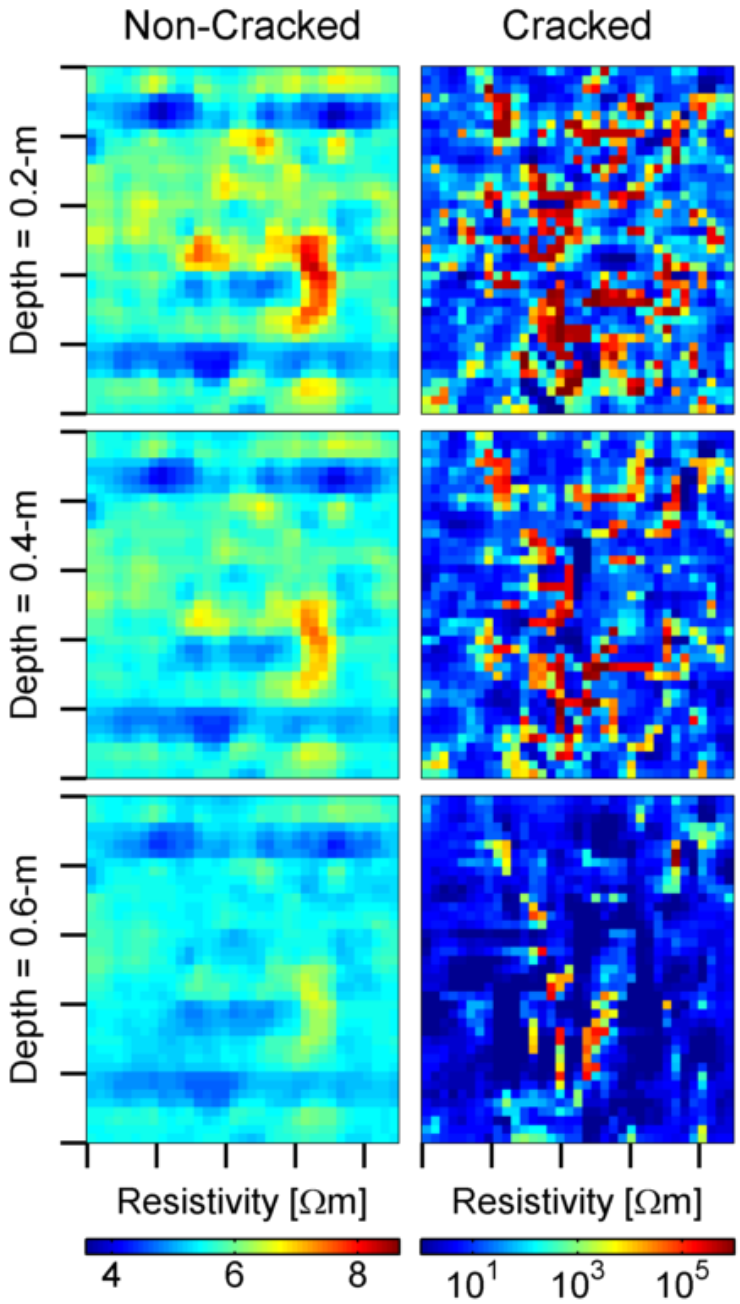

Figure 5. ERT electrical resistivity images with depth. Each of the images shows a 4.5 by 5 m horizontal slices though the three-dimensional inversion image. Data for the image of non-cracked soil was collected on April 20, 2012 and data for the image of cracked soil was collected on October 5, 2012. Black tick marks along image boarders denote 0.5-m increments. Note the difference in in range on scales of images from cracked and non-cracked soil

Soil water content within the experimental plot showed distinct spatial and temporal trends (Fig. 6a). In the spring months, soil profile was near field capacity. As the soil dried, the amount of water loss decreased with depth, as expected. For surface layers, measured water content declined to what would be expected if the soil were air-dry. For example, on September 13, the average water content at 0.2 m was 0.09 m^3m^{-3}, which corresponds to the soil equilibrated with a relative humidity of 0.6, as determined with a dewpoint potentiameter (model WP4, Decagon Devices Inc., Pullman, WA).

As the soil dried, an increase is the variability of soil water content was observed (Fig. 6b). This increase in variability was likely due, in part, to spatial variability in evapotranspiration (ET) across the plot. Variability in ET could have developed from the spatial structure in the distribution of shrubs and cracks, both which could increase localized ET. In addition to increasing ET, the presence of cracks in the zones of influence of the neutron moisture meter measurements, which was unaccounted for in neutron meter calibration, may have lowered water content predicted from measured count ratios. Because cracks were not distributed uniformly, this bias may have increased variability of soil water content.

As one would expect, as layer water content decreased, layer electrical resistivity increased (Fig. 6c). The greatest change in electrical resistivity was observed in the surface layers where change in water content was greatest. Between the measurements made under wet and dry conditions, electrical resistivity at 0.2-m depth increased by four orders of magnitude. Over the same time period, electrical resistivity remained nearly constant at 1.2-m depth.

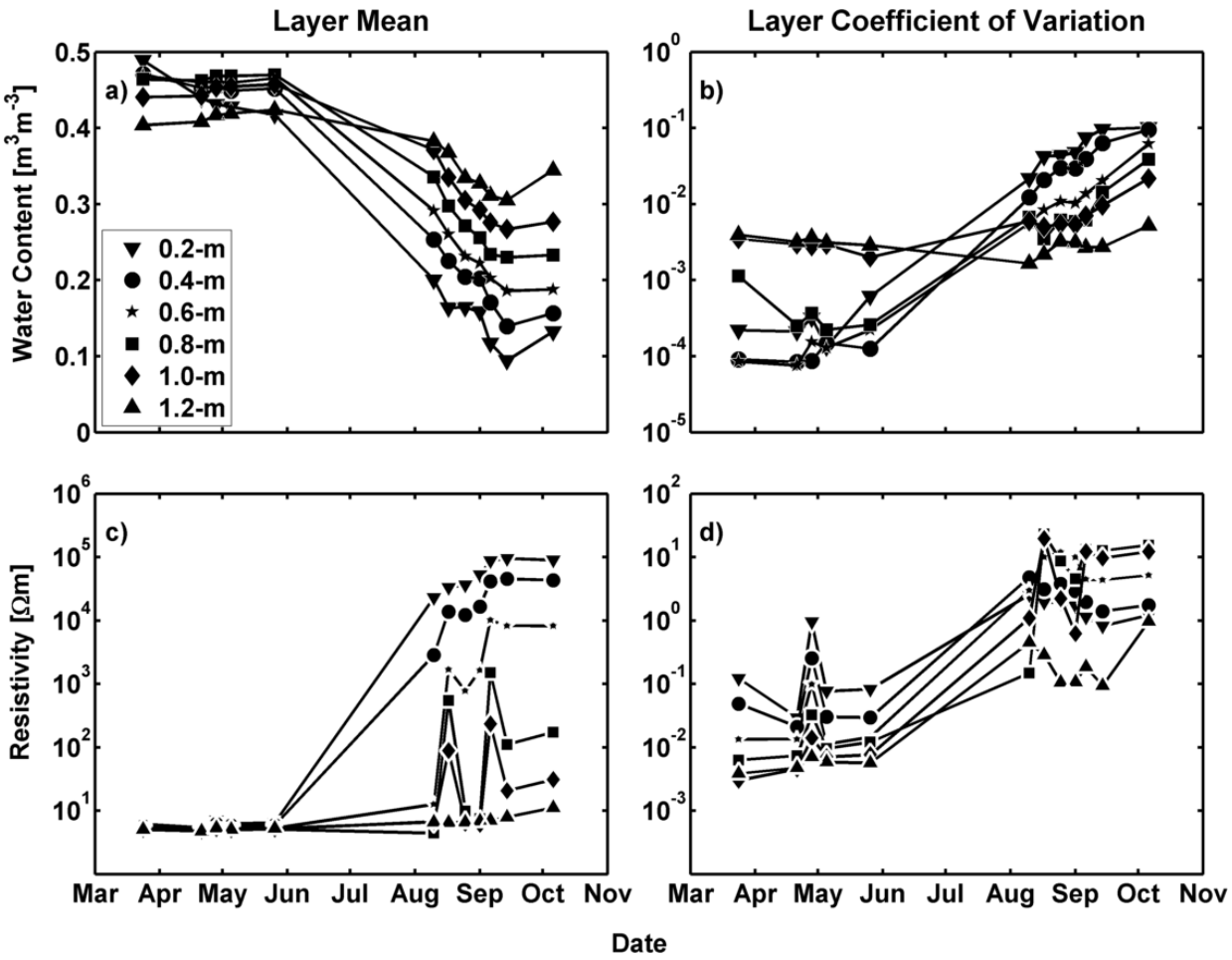

Figure 6. Temporal trends in water content and electrical resistivity, and their associated coefficients of variation. Water content data were the average of nine point measurements for each layer. Electrical resistivity data were layer averages interpolated from the three-dimensional ERT electrical resistivity map.

Layer electrical resistivity calculated from ERT also showed an increase in variability over the measurement period. As with water content, the greatest increases in variation were observed at 0.2-m depth and the least change in variation was observed at 1.2-m depth. During the driest periods, in the layers from 0.2 to 0.6-m depth, coefficient of variation of electrical resistivity was greater than one. This contrasts with soil water content, where for all depths the coefficient of variation was less than one. For electrical resistivity layers from 0.2 to 0.8-m depth, layer coefficient of variation exceeded the coefficient of variation of water content in the corresponding water content layer. This suggests that, at least for surface layers, electrical resistivity is much more variable than water content.

Comparison of Bulk Soil and Matrix Resistivities

For each soil moisture measurement, the radius of the sphere of influence was estimated using Eq. 5. Within each sphere, the mean electrical resistivity was then calculated from the three-dimensional electrical resistivity images to generate a volume-weighted bulk electrical resistivity for each soil moisture measurement ρ_{bulk} (Fig. 7).For non-cracked soil, ρ_{bulk} agreed well with ρ_{matrix}. Generally, ρ_{bulk} fell within the 95% prediction interval of laboratory data for cracked soil, a clear trend existed in the relationship of ρ_{bulk} with depth. For measurements at 0.2- to 0.8-m depth, ρ_{bulk} was appreciably greater than ρ_{matrix} (Fig. 7a-d). The poor agreement between field measurements on bulk soil and laboratory measurements on clods are most likely due to the effects that cracks have on the flow of current through the soil. This reason may explain the decrease in bias with depth. Soil shrinkage and crack formation associated

with loss of soil water loss (Fig. 7a) was greatest in surface layers. To quantify the bias between bulk electrical resistivity from ERT and matrix electrical resistivity from clods, the mean difference between ρ_{bulk} and ρ_{matrix} was calculated for each measurement depth (Table 3). For measurements made on non-cracked soil, results showed that bulk electrical resistivity was consistently lower than matrix resistivity resulting in negative bias. Additionally, the data demonstrated an increase in the magnitude of bias with depth, indicating that at deeper depths there was a greater discrepancy between bulk and matrix electrical resistivity. It is important to note that while biases showed a significant trend, the magnitude of biases for non-cracked soil is still less than the magnitude of error observed in laboratory measurements.

For measurements made between 0.2 and 0.6-m depths, bias observed in cracked soil was significantly greater than that observed in non-cracked soil. As with non-cracked soil, in cracked soil, bias decreased with measurement depth; however, in cracked soil the decrease in bias is much greater. In non-cracked soil, between 0.2m and 0.8m, bias decreased by 60%. Between the same depths in cracked soil, bias decreased by 99%. As mentioned earlier, the large bias in surface measurements of bulk electrical resistivity may be due to the presence of cracks. If this is the case, quantification of the bias between bulk and matrix electrical resistivity may provide an indirect method for identifying and mapping the degree of cracking under field conditions.

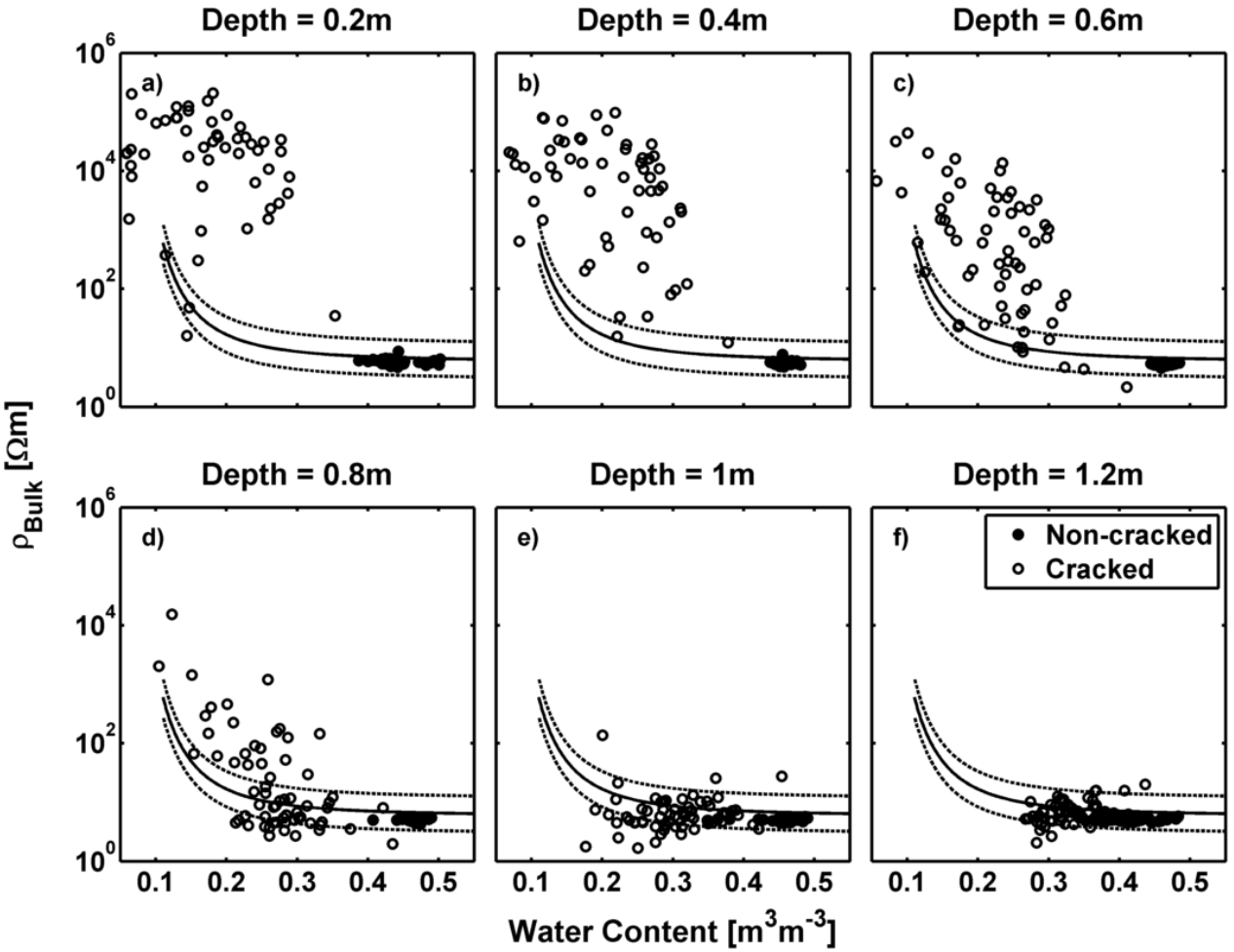

Figure 7. Bulk electrical resistivity vs. soil water content of non-cracked and cracked soil. The laboratory-calibrated model for electrical resistivity of the soil matrix is plotted along with the 95% prediction intervals (dashed lines)

Table 3. Mean bias between ρ_{bulk} and ρ_{matrix} for cracked and non-cracked soil. Positive bias indicated that ρ_{bulk} was greater than ρ_{matrix}.

	Mean Bias			
Depth	**Non-cracked Soil**		**Cracked Soil**	
--m--	----------Ωm----------			
0.2	-0.97	a†A‡	40400	aB
0.4	-1.16	aA	17100	bB
0.6	-1.45	bA	2800	cB
0.8	-1.56	bA	300	cA
1.0	-1.67	bcA	0	cA
1.2	-1.85	cA	-1	cA

†Means within the same column followed by the same lowercase letter are not significantly different (P<0.05, Tukey's HSD).
‡ Means within the same row followed by the same uppercase letter are not significantly different (P<0.05, Tukey's HSD).

Estimating Soil Water Content from ERT

The relationship of ρ_{bulk} from ERT to θ from neutron moisture meter was not well defined. The large uncertainty in ρ_{bulk} at any water content has important implications for use of ERT in mapping the physical state of soil. Typically, laboratory-determined relationships are used to estimate water content from measured electrical resistivity. For the data shown here, the large range in measured electrical resistivity when the soil was cracked would make accurate estimation of water content impossible, and when the soil was not cracked, the lack of sensitivity and relative degree of noise would make estimation of water content impossible (Fig. 8). However, it would seem possible that if water content could be independently measured in a scheme to map cracking, discrepancies between bulk electrical resistivity determined in the field and electrical resistivity of the soil matrix determined in the laboratory could be used to determine the degree of cracking. Field-scale maps of matrix resistivity could be

generated from maps of soil water content. Bulk resistivity could be measured using a mobile resistivity imaging system (Panissod et al., 1997). Comparison of the two maps could identify areas in the field of increased crack density or size.

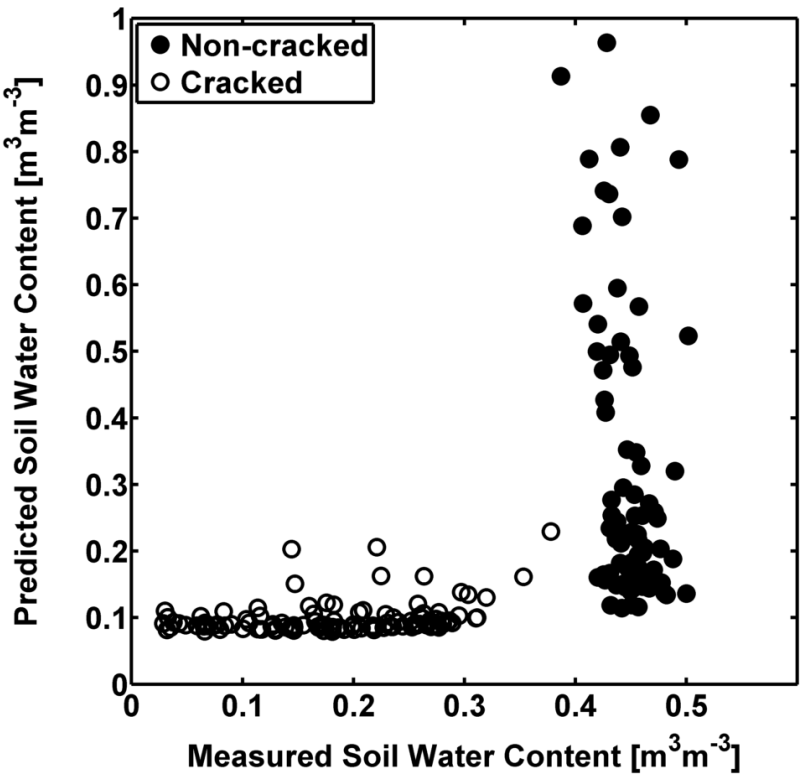

Figure 8. Water content estimated from the inverted laboratory-calibrated model plotted against water content measured from neutron moisture meter. Data were taken from 0.2 and 0.4-m depths.

CHAPTER III

MEASURING CRACK POROSITY USING THREE-DIMENSIONAL ELECTRICAL RESISTIVITY TOMOGRAPHY

Introduction

In Vertisols and vertic integrades, desiccation of the soil results in shrinkage of the soil matrix. The portion of total change in volume of the matrix that does not generate vertical shrinkage of the profile, results in increased porosity of the soil either in the form of soil cracks or inter-aggregate pores. Changes in soil porosity, particularly increases in crack porosity, can greatly alter the hydrology of a soil. Cracks have been shown to intercept and store runoff (Bouma, 1981) and increase evaporation (Ritchie and Adams, 1974). Despite the importance of cracks in the hydrology of Vertisols, little is known concerning the development and morphology of cracks.

Monitoring the development of crack porosity in Vertisols resulting from changes in soil water content is challenging as cracks and inter-aggregate pores are difficult to measure. Infilling cracks with sand or paraffin has been used to measure crack volume (Dasog and Shashidhara, 1993; Peng et al., 2006). Once cracks are infilled, the soil can be excavated and the subsurface distribution of cracks can be mapped. Infilling methods can provide accurate, direct measurements of crack porosity but are tedious and cannot be used to monitor temporal changes in crack porosity. One non-destructive method that might be of use is electrical resistivity tomography (ERT). With ERT, a current of known amperage is allowed to flow through the soil between two

electrodes generating an electric field within the soil. Using a separate pair of electrodes, voltages within the electric field are measured. By systematically moving the source and sensing electrodes across the surface of the soil, it is possible to generate a three dimensional representation of the structure of the subsurface. While ERT has been shown to be sensitive to cracks under laboratory conditions (Samouëlian et al., 2003, 2004; Sentenac and Zielinski, 2009; Greve et al., 2010b) and in the field (Amidu and Dunbar, 2007; Greve et al., 2010a), no studies have related ERT data to direct measurements of crack porosity.

A major constraint of ERT lies in the fact that the resolution of the representation of the subsurface is limited by the spacing between electrodes across the surface (Samouëlian et al., 2005). For cracks that may be only a few centimeters wide, resolving individual cracks using ERT would require electrode spacing on the order of centimeters. Such small electrode spacing would require an impractically dense array of electrodes and would limit the area and depth over which measurements could be made. To measure cracks at any appreciable depth and over any practical area, electrodes need to be spaced much further apart; on the order of 0.5 m. At this electrode spacing, resolving individual cracks is impossible, however, it is clear that the presence of crack affects the bulk electrical resistivity of the soil and therefore it may be possible to use ERT to measure cracks in a bulk sense. The objective of this study was to investigate the accuracy and limitations of ERT as a tool for nondestructive monitoring of soil crack porosity under field conditions.

Materials and Methods

Field Study Site

A field site for ERT and crack porosity measurements was located near Bryan, TX (30° 37’ 54.8’’ N, 96° 28’ 59.1’’ W). The soil is Burleson clay, a fine smectitic thermic, Udic Haplustert (Soil Survey Staff, 2012), the slope was less than 0.01 m m^{-1} and there was no evidence of gilgai microtopography. The site was fenced for pasture but had been left ungrazed for several years prior to the study. A 4.5 m by 5 m study plot was located at the site in an area with uniform vegetative cover and evidence of shrinkage and swelling in the forms of open cracks and scars from previous cracks. On a roughly weekly basis between April and October of 2012, soil water content within the plot was measured. At the end of the study period, an ERT survey of the plot was conducted. Following the ERT survey, crack porosity within the plot was also measured (see later discussion).

Electrical Resistivity Tomography

On October 5, 2012, when the soil was seasonally dry and large cracks were present, an ERT survey of the study plot was conducted using an AGI Supersting R8 resistivity/IP meter (Advanced Geosciences Inc., Austin TX). Data were collected using a dipole-dipole array at the soil surface. The array consisted of 9.5-mm diameter stainless steel rods, positioned in a 10 by 11 grid with 0.5-m spacing. After the survey was completed, survey data were analyzed using the inversion software, EarthImager3D (Advanced Geosciences Inc., Austin TX). In an ERT inversion, the inversion software uses surface measurements to produce an image or representation of the subsurface

electrical resistivity. The inversion software generates this image by finding the set of subsurface electrical resistivities that can accurately reconstruct of simulate the observed survey data. For this study, we collected data using a two-dimensional array allowing the inversion software to generate a three-dimensional representation of the subsurface.

Table 4. Inversion parameters

Parameter Name	Description	Values
Initial Lagrange Roughness	Constrains model roughness, higher values allow for rough models with low RMS and low values provide smooth models with higher RMS	5, 10, 50, 100, 500, 1000, 5000
Horizontal/Vertical Roughness Ratio	Weights the model roughness constraints to either vertically or horizontally. Values below 1 have preference for horizontally layered models with values above one preferring vertically contrasting models	1, 1.5, 2, 2.5, 3, 3.5, 4
Maximum Electrical Resistivity [Ωm]	The maximum electrical resistivity an inversion model element is allowed to achieve	10^{1}, $10^{1.5}$, 10^{2}, $10^{2.5}$, 10^{3}, $10^{3.5}$, 10^{4}

In the inversion software, several parameters constrain or guide the inversion. Changes in the values of these parameters effect the way the software searches for the optimum representation of the subsurface resistivity, and can yield appreciably different representations from the same survey data. To determine what effect these inversion parameters have on the representation of the subsurface electrical resistivity, field data were inverted multiple times using different combination of parameters. For this analysis three parameters were selected. For description of each parameter and the

values it was assigned, see Table 4. For the remainder of the discussion, we will refer to unique combinations of inversion parameters as an inversion setting. Every possible combination of parameter in Table 4 was investigated with each of the inversion settings resulting in a unique representation of the subsurface resistivity.

To represent the electrical resistivity of the subsoil, the inversion software uses a three-dimensional finite element mesh where each element is assigned an electrical resistivity. The inversion routine searches for the set of electrical resistivities of the elements that generate the closest fit to the surface survey data. In the horizontal plane, elements were arranged in a 36 by 40-element rectangle to represent the 4.5 by 5-m study plot. The sides of each element were 0.125 m in length. Vertically, elements were arranged in seven layers centered on 0.06, 0.21, 0.38, 0.57, 0.78, 1.04, and 1.33-m depth. Due to the decreasing resolution of ERT with depth and to save computational time, the thickness of elements in each successive downward layer increased.

Estimating Total Porosity Generated by Shrinkage

Following Bronswijk (1989), the total change in soil volume ΔV was equated with the total volume of water loss ΔW. As the soil shrank, a portion of the total shrinkage was partitioned into vertical shrinkage Δz. If shrinkage was isotropic, vertical shrinkage can be closely approximated by: $\Delta z = 1/3\ \Delta V$. These estimations can be valid only if the soil water content is above the shrinkage limit. Below the shrinkage, additional loss of soil water does not result in additional soil shrinkage (Olsen and Haugen, 2007). Bovin et al. (2007) showed that soil cores from Texas Vertisols exhibit isotropic shrinkage. The remaining two-thirds of the volume change occurred

horizontally and contributes to an increase total shrinkage porosity $\Delta\boldsymbol{\phi}$. One can further partitioned total shrinkage porosity into that generated by cracks and that generated by an increase in inter-aggregate porosity. Bronswijk (1989) assumed that crack porosity equaled total shrinkage porosity.

Using this framework, it was possible to estimate total shrinkage porosity from measurements of soil water loss. For this study, soil water content was measured using a neutron moisture meter. To facilitate neutron moisture meter measurements, nine access tubes were installed on a 2-m grid. To install an access tube, we extracted a 31.4-mm diameter core to a depth of 2.1 m using a hydraulically drive probe (Giddings Machine Company, Windsor, CO). The hole left from the core was then enlarged using a 50.8-mm diameter auger. Finally, 50.8-mm diameter, Schedule 20 PVC tubes were inserted into the holes. Additional neutron access tubes were installed outside the plot area to facilitate calibration of the meter. At the calibration access tubes, count ratios of thermalized neutrons to those from the instrument standard were recorded with depth. Four soil cores, 38.1 mm in diameter, were extracted from within 0.1 m of the tube and determined the volumetric soil water contents of core segments by mass loss on oven drying at 105 °C and the volume of a core segment. To cover the range of observable soil moisture contents in the field, this calibration procedure was conducted twice; once when the soil was near field capacity and again when the soil was seasonally dry. For each calibration sampling, a new access tube was installed on undisturbed soil. Using wet and dry calibration data a linear equation was found relating water content to count ratio. At each access tube at thee study site, count ratios were measured every 0.2 m

from 0.2 to 1.8 m below the soil surface. Measured count ratios were then converted to soil water content using the calibration equation. Measurements were made on a roughly weekly basis from the seasonal maximum soil water content in April until the time of crack in-filling and excavation in October.

From soil water content measurements made with the neutron moisture meter, shrinkage of soil in the study plot was estimated using maximum observed water contents at given depths as references. At the initial soil water content measurement $i = 0$, the soil profile is considered to be composed of nine 0.2-m thick layers between 0 and 1.8 m. For an individual soil layer k, the upper depth of the layer at time i, is denoted by $z_{k,i}$ with the thickness of the layer equal to the difference between the upper depth of the layer and the upper depth of the adjacent layer, $k+1$. Soil water content at time i, was measured at depths $z_{m,i}$. Measurement depths were located relative to the soil surface on 0.2-m intervals from 0.2 to 1.8 m depth. On measurement date $i = 0$, layer depths and soil water content measurement depths were equal, i.e. $z_{k,i=0} = z_{m,i=0}$ for all $k = m$. However, as the soil shrank, layer depths and measurement depths no longer aligned. To account for the effects of changing layer thickness relative to the fixed intervals on which soil water content was measured; we interpolated layer water content from measured soil water content using a spline function:

$$\theta_{est}(z_{k,i}) = f\left(\theta_{m,i}, z_{m,i}\right) \quad [18]$$

where $\theta_{est}(z_{k,i})$ is the estimated soil water content (m^3m^{-3}) of layer k at time i. The spline function f, used thought this study was the cubic smoothing spline packaged with MATLAB (2012b, MathWorks, Natick MA). Observed water content $\theta_{m,i}$, was

generated from neutron moisture meter measurements made at depth $z_{m,i}$. Soil water content above 0.2 m, and therefore outside the interpolation range of *f(z,i)*, was considered constant and equal to water content measured at 0.2 m. Soil water content of layer *k* at measurement date *i* was calculated as:

$$W_{k,i} = \int_{z_{k,i}}^{z_{k+1,i}} f\left(\theta_{m,i}, z_{m,i}\right) dz \quad [19]$$

where $W_{k,i}$ is the depth of stored water, in m^3m^{-2}. Between two adjacent dates, *i* and *i-1*, the change in layer thickness of layer *k* was calculated using:

$$\Delta z_{k,i} = r\left(W_{k,i-1} - W_{k,i}\right) \quad [20]$$

where *r* is the ratio of vertical to total shrinkage. For this study, shrinkage was assumed to be isotropic and therefore, *r*=1/3 (Bronsjizk, 1990).

At soil water content below a critical value known as the shrinkage limit, additional water loss does not result in additional shrinkage and increased crack and inter-aggregate. To account for this, when layer water content was lower than the shrinkage limit, *r* was changed from 1/3 to zero. For this study, the shrinkage limit was assumed to equal 0.18 m^3m^{-3}. This estimate of the shrinkage limit was based on measurements of soil water content and electrical resistivity made on intact soil cores. As the cores dried, their electrical resistivity remained relatively constant until their water content reached about 0.18 m^3m^{-3}. At this point, the electrical resistivity of the soil increased rapidly (see Chapter II). This rapid increase in electrical resistivity was attributed to desaturation of the soil pores (Lesch and Corwin, 2003) and indicated that the water content of the soil had dropped below the shrinkage limit (Olsen and Haugen, 2007).

Without independent measurements of soil subsidence, layer depths at time *i*, were unknown for all measurements except measurements at *i = 0*. To account for this, layer elevations starting with measurement *i = 1* were estimated from estimated layer shrinkage. For these estimations, we adopted the following iterative procedure.

1. For measurement date *i*, soil water content was estimated for each layer *k* assuming no shrinkage between measurements (i.e., $z_{k,i} = z_{k,i-1}$)

$$W_{k,i} \approx \int_{z_{k,i-1}}^{z_{k+1,i-1}} f\left(\theta_{m,i}, z_{m,i-1}\right) \quad . \qquad [21]$$

   Note that layer and measurements depths were taken from the previous measurement date, *i-1* but measured soil water content was taken from the current measurement date *i*.

2. Next, layer shrinkage between measurements *i* and *i-1*was approximated as:

$$\Delta z_{k,i} = \mathrm{r}\left(W_{k,i-1} - W_{k,i}\right) \qquad [22]$$

3. With estimated layer shrinkage, updated layer depths were estimated using:

$$z_{k,i} = z_{k,i-1} - \sum_{p=k-1}^{p=n} \Delta z_{p,i} \qquad [23]$$

4. Neutron moisture meter measurement depths were also adjusted soil water content measurement depths for total profile shrinkage by:

$$z_{meas,i} = z_{meas,i-1} - \sum_{p=1}^{p=n} \Delta z_{p,i} \quad [24]$$

5. Using the updated layer and measurement depths for date *i*, layer water content was recalculated as:

$$W_{k,i} \approx \int_{z_{k,i}}^{z_{k+1,i}} f\left(\theta_{meas,i}, z_{meas,i}\right) \quad [25]$$

   Note that unlike in Eq. 21, the layer and measurement depth indices match the water content depth indices.

6. Steps 2-6 were iterated until the change in total profile shrinkage between successive iterations was less that 0.1%. Typically convergence was achieved within three to five iterations.

Using this procedure, layer depth and water content were estimated for all measurement dates. For each layer, layer shrinkage porosity $\Delta\phi_{k,i}$ could be calculated from:

$$\Delta\phi_{k,i} = 1 - \left[1 - \left(\theta_{k,max} - \theta_{k,i}\right)\left(r^{-1} - \theta_{k,i}\right)^{-1}\right]^2 \quad [26]$$

where $\theta_{k,max}$ is the maximum water content of layer *k* over all measurement dates. If $\theta_{k,i}$, was below the shrinkage limit, the value of $\theta_{k,i}$, was replaced with the water content at the shrinkage limit, 0.18 m^3m^{-3}. This adjustment prevented overestimating layer shrinkage porosity, due to soil water loss below the shrinkage limit.

Measuring Porosity Generated by Cracks

The day following the ERT survey soil cracks were filled with a 1:1 by volume mixture of white Portland cement and water. This ratio proved fluid enough to run easily into cracks yet contained enough cement to properly cure. White cement was used because it provided a high contrast with the soil. A small amount of dish soap (<1% by volume) was added to entrain air in the mixture making it weaker and easier to excavate. Using a backhoe equipped with a toothless bucket, soil was excavated to expose surfaces from 0.25 to 1.5-m depth, in 0.25-m increments. While care was taken to keep the depth of excavation constant, the final depth varied approximately 0.1 m above and below the targeted depth. After a layer was excavated, loose soil was removed from the exposed surface using hand trowels, brushes, and a leaf-blower. Next, a 0.5-m spaced grid of reference pins was placed on the layer surface. Using a digital camera, sections of the soil surface were photographed. To keep the camera stable and oriented roughly perpendicular to the soil surface, it was mounted on a boom attached to a tripod. Each photograph covered slightly over 1 m^2 of soil surface and contained 9 reference pins. Adjacent photographs overlapped slightly so that they contained three of the same reference pins (Fig. 9). For each layer, a set of 25 images was sufficient to cover the entire plot.

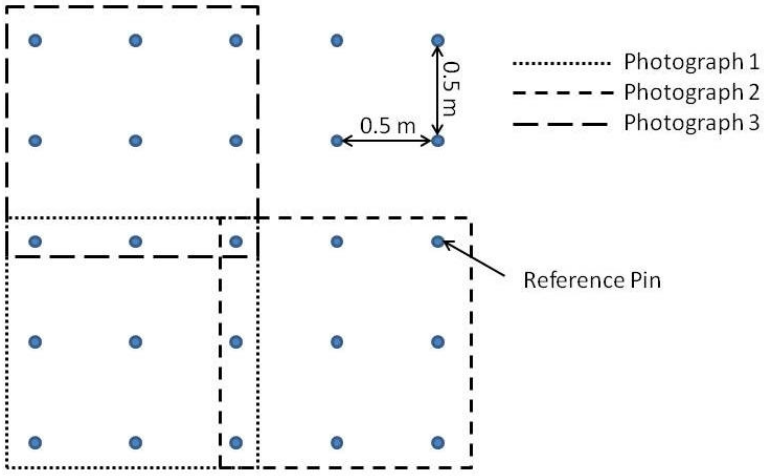

Figure 9. Schematic of soil layer photographs and reference pins.

Photographs were processed using MATLAB (2012b, MathWorks, Natick MA). First individual photos were cropped to contain only nine reference pins. Then, the location of the reference pins within each photo were found and used to correct photos for lens tilt and distortion. These corrections allowed neighboring images to be aligned. Next, each photo was transformed into a binary image in order to delineate cement and cement filled cracks from the soil background. Due to differences in brightness and contrast between images, a single color or gray-scale threshold could not be applied uniformly to all images. Instead, a K-means algorithm was used to segregate the image into three regions based on the pixel color (MathWorks, 2012). One region contained the white pixels of cracks and any residual cement pieces. The second region contained the gray soil background. The final region contained black pixels near the image boarder generated through tilt and distortion correction. For some images in the 1.25

and 1.5-m layers, where the number of white pixels was small, more k-means regions were added to segregate white pixels from light gray soil. When additional regions were used, it was assumed that all the cracks were contained in the region with the highest mean pixel value, and therefore the region with an average color closest to white.

Once photos were converted to binary images, all 25 images taken at a single excavation depth were combined into a mosaic. Mosaics were then cropped to match the extent of the 4.5 by 5 m plot. Final images were 9000 by 8100 pixels with a resolution of 3.2 mm^2 per pixel. We then applied a moving average filter to each mosaic. The moving average filter removed all isolated groups of white pixels smaller than 25 pixels. This filter was applied to remove any small patches of cement that were not removed prior to photographing the soil. The filter may have removed some of the small cracks from the layer images however compared to larger cracks, the smallest cracks likely contributed much less to the increase in bulk soil electrical resistivity. Comparisons between crack porosity and electrical data were made using filtered and non-filtered images. In all cases, filtered images provided higher accuracy models and therefore we will restrict discussion to filtered images.

To facilitate comparisons with ERT data, crack layer images were segregated into small square regions. Within each region, crack-generated porosity was calculated (hereafter, crack porosity) as the ratio of crack area to the area of the region. Each region covered the same area as a single element in the ERT inversion mesh. Regions were aligned so that the center of each region shared x-y coordinates with the centroid of an element in the ERT inversion mesh. Using the method, the electrical resistivity and

crack porosity of the soil were represented on a single reference grid of square regions. Each cell within the grid was associated with seven electrical resistivities and six crack porosities; one resistivity for each depth in the inversion mesh and one crack porosity for each crack layer image. With all analyses in this study, crack porosity and electrical resistivity were paired by cell within this reference grid. For example, if crack porosity data from the 0.25 m layer were regressed with electrical resistivity from 0.57 m, each resistivity/porosity data pair would consist of data from different depths but within the same cell of the reference grid (i.e., have different depths but the same x-y coordinate). For all analysis, data from within 0.5 m of the plot edge was excluded in order to avoid edge effects.

To successfully invert electrical resistivity data, a very small inversion mesh was needed. This mesh however, is still too coarse to identify individual cracks. The effect of cracking on soil electrical resistivity is likely spatially diffuse. The effect of a single crack cannot be isolated to a single cell in the inversion mesh but rather affects all the cells within a region surrounding the crack. To account for this, the relationship between bulk soil electrical resistivity and crack porosity was analyzed at several neighborhood or region sizes. To generate data on different neighborhood sizes, crack porosity and electrical resistivity data were averaged within progressively larger region sizes. Within each neighborhood size class, regions consisted of horizontal, non-overlapping squares. For the regions in the smallest analysis scale, regions were defined by the squares of the reference grid. For each progressively larger analysis scale, region size was increased by 0.125 m or the equivalent of one square in the initial reference

grid. As region size increased, crack porosity and electrical resistivity were represented by fewer and fewer individual regions. This decrease in sample size led to a decrease in resolution but also functioned to smooth out small scale fluctuations in the data and better represent the diffuse nature of the relationship between crack porosity and bulk electrical resistivity.

Determining Optimum Inversion Settings

Before ERT can be a used to measure crack porosity, the optimum ERT inversion setting needed to be identified. The optimum inversion setting would yield the most accurate estimation of crack porosity. There are two approaches to identifying the optimum ERT inversion settings. The first approach was to find the inversion setting that provides ERT data that was most correlated to crack porosity. The resulting inversion setting provided the most accurate predictions of crack porosity for a given neighborhood size. One issue with this approach is that the optimum inversion settings are specific to one particular soil, taken at one stage of cracking, and averaged within one neighborhood size. There was no guarantee that these settings provided useful data for different soils, with different crack patters or averaged within different neighborhood sizes. An alternative approach, and the one that was adopted in this study, was to identify a generalized inversion setting, one that performed well across a range of soils or neighborhood sizes. To do this data from each inversion setting was analyzed at region sizes. Within each region size class, inversion settings were ranked by their correlation to crack porosity. The most commonly used parameter levels from the highest ranked inversion settings were identified. The primary assumption here was that

by identifying the inversion parameters that all well correlated models share, it would be possible to find an inversion setting that would perform well under a range of conditions and not just on specific soil or scale. Although we could no test if the generalized inversion will perform well on soils with different cracking patterns, we can determine how well it performs across a range of neighborhood sizes on the soil in our study site

To identify the generalized inversion setting, inversion settings were ranked by cumulative, maximum correlation coefficient (CMCC). For each inversion setting, eparate CMCC's were calculated for crack porosity and ERT data averaged on each region size. To calculate the CMCC, correlation coefficients between electrical resistivity and crack porosity data were calculated. Due to poor correlation with electrical resistivity, crack porosity data from 1.25 and 1.5 m was omitted from analysis. Separate coefficients were calculated for each possible combination of electrical resistivity and crack porosity measurement depths. Therefore, in the resulting data, each of the four remaining crack porosity measurement depths was associated with seven correlation coefficients, one for each electrical resistivity measurement depth. Across all electrical resistivity measurement depths and within each crack porosity measurement depth, the maximum absolute correlation coefficient a was identified. Correlation coefficients were calculated using electrical resistivity and log normalized electrical resistivity. Similar results were found using both normalized and non-normalized data. For the sake of discussion, only results from the original, non-normalized data will be discussed. CMCC was then calculated as the sum of the maximum absolute correlation coefficient s across all crack porosity measurement depths. Correlation coefficients that

were not significant at the 95% confidence level were omitted. Inversion settings with the highest CMCC resulted from electrical resistivity data that were most correlated to crack porosity between 0.25 and 1 m.

A limitation of this analysis is that for CMCC's calculated for crack porosity measurement depth, correlation coefficients calculated using data from only one electrical resistivity depth were considered. Due to the spatially diffuse effects of cracking on electrical resistivity it is very likely that a single crack influences the electrical resistivity at several depths. To test this, a multiple linear regression was fitted to electrical resistivity data where crack porosity at one depth was considered to be a liner combination of the electrical resistivity at all seven electrical resistivity depths. Such models proved fruitless because the influence of most electrical resistivity depths on predicted crack porosity was insignificant. When insignificant terms were removed from the model, crack porosity could be successfully predicted using data from only one electrical resistivity depth.

Results and Discussion

Crack images (Fig. 10) showed similar patterns across depths. In many of the crack layer images, large cracks were present in the same locations. For example, the crack denoted by the arrow in Figure 10 was visible in all crack images from 0.25 to 1 m depth. This crack appears to be a single, continuous crack that extends through most of the soil profile. Many of the large, thick cracks exhibit a similar pattern, cutting across many image depths. Cracks were also well connected horizontally. It is possible to

trace a continuous path within the crack network from one side of the plot to the other. Large continuous crack present a significant barrier to electrical current flow, forcing current to run below or around cracks and likely contribute substantially to increased electrical resistivity of the bulk soil.

Shrinkage Generated Porosity

Layer water content measured on the day of the ERT showed increased soil water content with depth (Fig. 11). Much of the soil in the upper three layers had water content below the shrinkage limit and had therefore reached a point of maximum shrinkage. Compared to layer water content on the day of the ERT survey, layer maximum water content demonstrated a trend of decreasing water content with depth. Within each layer, the variability of maximum water content was much lower than variability at the time of the ERT survey. This suggests that any observed variability in shrinkage porosity or crack was the result of variability in drying of the soil rather than variability in initial soil water content of each layer.

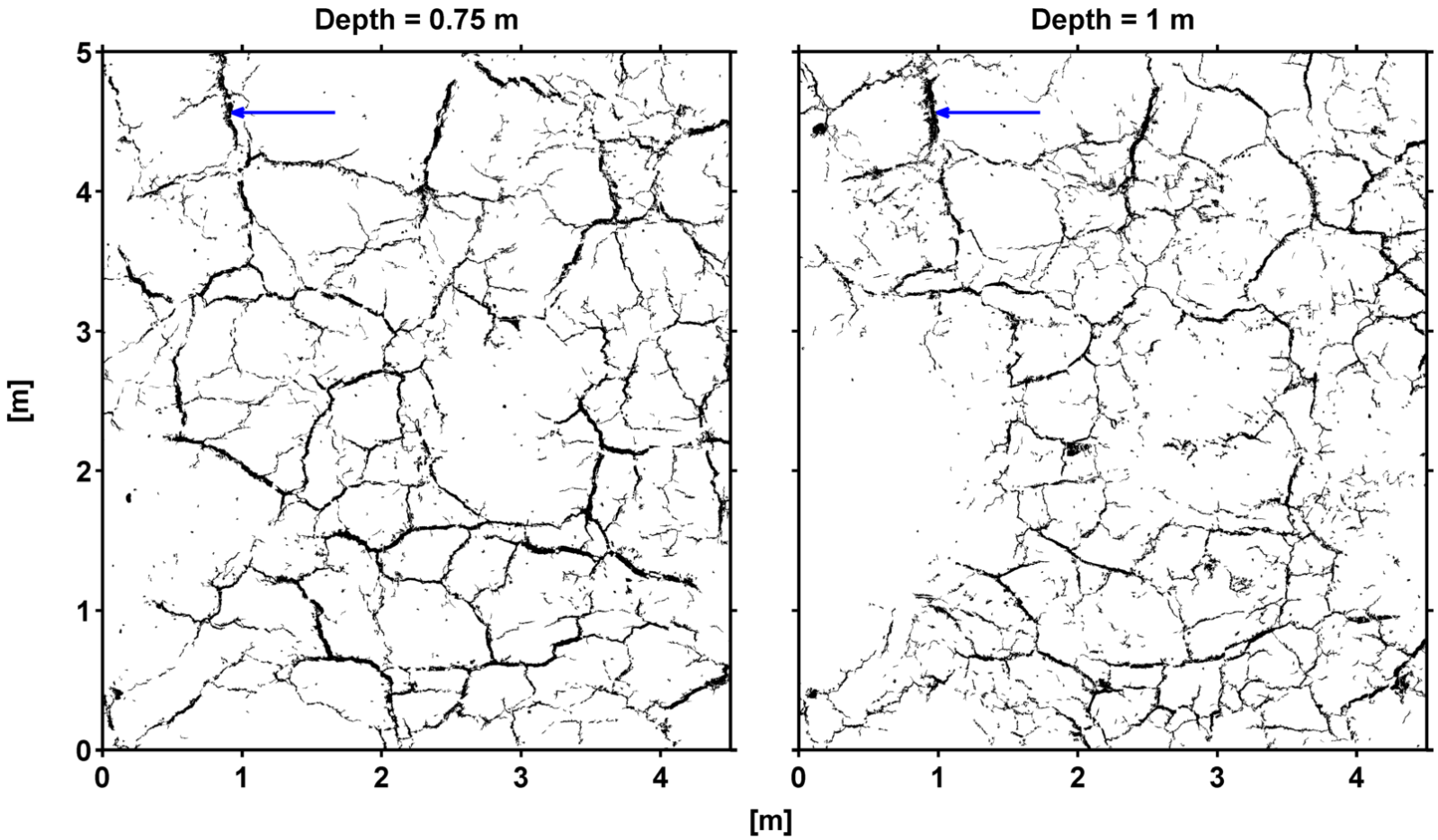

Figure 10. Crack pattern from two layer mosaics

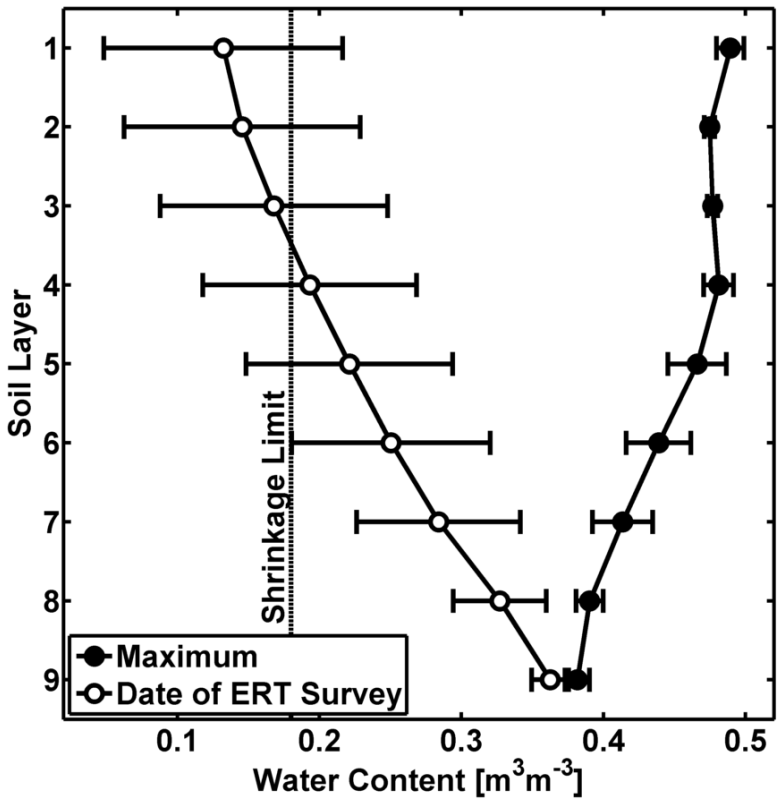

Figure 11. Average soil water content by layer. Open circles represent data from the day of the ERT survey. Closed circles represent maximum observed layer water content during the study. Horizontal error bars represent the 95% confidence intervals of layer means.

Total shrinkage porosity showed a decreasing trend with depth (Fig 12). Crack porosity measured from excavation images was nearly constant between 0.25 and 1-m depth. Below 1-m, crack porosity began to decrease. For crack images above 1-m depth, crack porosity was significantly less than total shrinkage porosity, lying outside the 95% confidence interval of layer means. Several explanations exist for this discrepancy. Firstly, our method of filling cracks may have under represented crack porosity if cement did not penetrate some of the cracks either because they were not connected to the main

crack network or were too small for cement to flow easily into the cracks. In the greater scope of this project, these concerns may not be relevant because isolated or very small cracks likely contributed little to increases in bulk soil electrical resistivity compared to large well connected cracks. Additionally when compared to cracks connected with other cracks or the surface, isolated cracks may not be as relevant to the hydrology of vertisols. If this is true, the omission of isolated cracks from analysis would have little impact on the interpretation of results from a hydrological standpoint.

Another explanation for this discrepancy is that soil layer shrinkage did not occur according to the 1:3 ratio suggested by Bronswijk (1989). Dinka et al. (2013) found that when layer shrinkage was measured in the field, the ratio of soil water loss to layer shrinkage was less than 1:3. If this was also the case, then Eq. 20 and 22 likely overestimated layer shrinkage. Overestimating layer shrinkage would have resulted in underestimation of layer thickness and water content. Underestimation of layer water content would result in an overestimation of crack porosity (Eq. 26).

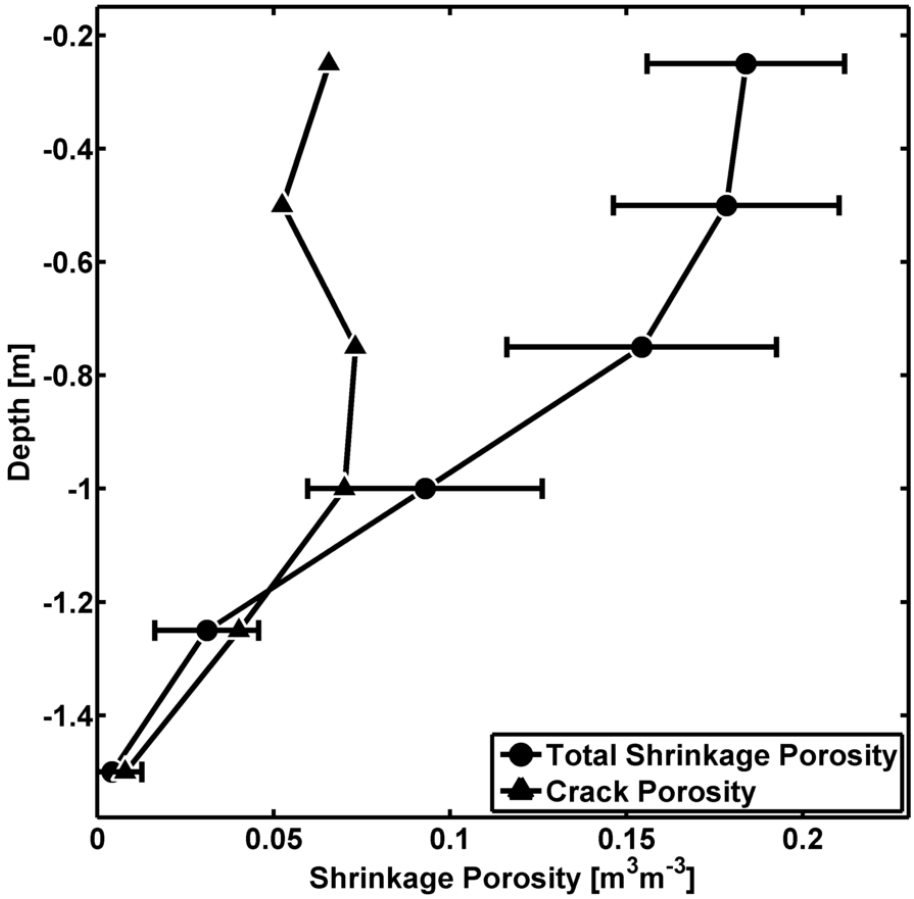

Figure 12. Increase in porosity predicted from Eq. 26 plotted versus depth. Error bars represent the 95% confidence intervals around the layer mean.

It is possible, and likely, that only a portion of total predicted shrinkage is partitioned into the formation of cracks. The remaining fraction of total soil shrinkage contributed to the formation of inter-aggregate or intra-aggregate pores. The surface of the Burleson soil at the time of infilling was crumbly in nature, which suggests that there was a considerable amount of inter-aggregated pores generated by shrinkage.

Understanding the partitioning of total porosity into various scale-depended components is critical for flow of water, gases, and energy in Vertisols.

Bulk Electrical Resistivity and Crack Porosity

We ranked inversion settings from each region size by CMCC. From the upper quartile of ranked inversion settings and for each region size, we calculated the relative frequency of each parameter value for all inversion parameters (Table 5). The parameter values of the generalized inversion setting consisted of parameter values with the highest average relative frequencies across all measurement scales. Based on these averaged frequencies, we identified the generalized inversion setting as having an initial LaGrange roughness (LR) of 100, a horizontal/vertical roughness ratio (HV) of 2.5, and a maximum electrical resistivity (MR) of 10^2 Ωm .

The ability of CMCC to discriminate between parameter values appeared to be different for each inversion parameter. For example, with MR, at all but one region size, the same parameter value, 10^2 Ωm was most frequent. This resulted in a well-defined maximum average frequency of 59% for the parameter value of 10^2 Ωm. This maximum average frequency was substantially larger than the next highest frequency of 21%. However, the maximum average frequency was not as well defined for the other parameters. With HV, maximum average frequency was only 16% with a lowest average frequency of 12%. Such a small range in average frequency resulted in a more poorly identified maximum. These results may indicate that the correlation between bulk electrical resistivity and crack porosity is more influenced by some inversion parameters

Table 5. Relative frequency of each inversion parameter level. Data include only upper quartile of CMCC ranked inversions from crack porosity from 0.25 to 1 m. Maximum percentages for each region size are bold.

	Region Size								
	----------m^2----------								----
Inversion Parameter	0.02 (n=30)	0.06 (n=31)	0.14 (n=29)	0.25 (n=24)	0.39 (n=27)	0.56 (n=21)	0.77 (n=31)	1 (n=29)	All
Initial Lagrange Roughness	----------%								
5	12	8	12	0	0	19	8	0	7
10	12	10	12	9	4	19	0	2	8
50	12	10	16	9	16	17	30	2	14
100	17	18	**18**	20	**25**	**42**	**36**	6	**23**
500	**20**	**20**	12	**22**	24	3	8	**38**	18
1000	15	16	14	**22**	16	0	15	29	16
5000	13	18	16	20	16	0	3	23	14
Horizontal/Vertical Roughness Ratio									
1	12	10	14	7	**24**	6	13	15	12
1.5	12	15	**16**	9	18	6	13	17	13
2	13	15	14	11	16	19	**18**	**19**	**16**
2.5	15	13	**16**	17	8	**28**	13	17	**16**
3	15	15	14	**26**	12	17	15	4	15
3.5	**17**	**16**	12	13	12	17	10	13	14
4	**17**	**16**	14	17	12	8	**18**	13	15
Maximum Electrical Resistivity [Ωm]									
1	0	0	0	0	0	0	0	0	0
1.5	0	0	0	0	0	0	0	0	0
2	**82**	**74**	**84**	**61**	**57**	**61**	**36**	15	**59**
2.5	18	23	16	20	31	11	13	**33**	21
3	0	3	0	15	8	8	21	21	10
3.5	0	0	0	4	2	8	16	15	6
4	0	0	0	0	2	11	13	15	5

than by others. Particularly, anisotropy (HV) and roughness constraints (LR) may not play as important a role in inversion of crack soils as does MR.

Considering that air-filled cracks have essentially infinite electrical resistivity, it was surprising to find that in the generalized inversion setting, maximum electrical resistivity is quite small. From the data shown here, bulk electrical resistivity is most correlated with cracking when electrical resistivity of the inversion mesh is constrained to 100 Ωm. Electrical resistivity measured on intact soil clods showed that, in the absence of cracks, Burleson clay can reach electrical resistivity of 100 Ωm when the water content is 0.15 m^3m^{-3}. This suggests that when the electrical resistivity of the soil is averaged over appreciable volumes, the effect of cracking is of similar magnitude to the effect of water content loss. It is important to note that in all inversion settings, minimum electrical resistivity was fixed at 5 Ωm. This was the minimum electrical resistivity measured on intact soil clods.

While the parameter values used in this study are not directly transferable to other inversion software, they can serve as a guideline for other studies. Based on the generalized inversion setting found here, for the best correlation between ERT data and crack porosity, inversion settings should constrain inversion to smooth models with a limited electrical resistivity. These results also show that maximum electrical resistivity appears to be particularly important in producing ERT data that is well correlated to crack porosity.

Using electrical resistivity data from the generalized inversion setting, linear models relating crack porosity, ϕ_{crack}, and bulk electrical resistivity, ρ_{bulk}, were fitted.

$$\phi_{crack} = \beta_0 + \beta_1 \rho_{bulk} \quad [27]$$

where β_0 and β_1 are the intercept and slope terms respectively. We fitted separate models for each crack porosity depth and region size. For each crack porosity measurement depth and region size, the electrical resistivity data used in model parameterization were taken from the electrical resistivity depth with the highest correlation to crack porosity. R^2 and root mean squared error (RMSE) were calculated for each model. We also calculated model parameters, R^2, and RMSE using electrical resistivity data from all other inversion settings. Models that were not significant at the 95% level were omitted. Accuracy and goodness of fit from all significant models were compared to those from the generalized inversion model (Tables 6 and 7).

Results showed that models calibrated using data from the generalized inversion model (henceforth generalized models) preformed fairly well at most region sizes and depths. Region sizes at which the generalized inversion model performed poorly were the largest two region sizes, 0.77 and 1 m^2. At these region sizes, the total number of all inversion settings with significant models was smaller. As the region size becomes larger, each depth layer is covered by fewer regions leading to a decrease in the number of data used to fit each model. This decrease in number of significant models is likely due to the much smaller sample size at large scales. Including the largest two region sizes, the R^2 of the generalized inversion model, on average, fell within the upper 72% of models. Excluding the largest two models, this percentile increases to 82%. One issue with using linear models is that crack porosity and electrical resistivity data are spatially autocorrelated. Spatial autocorrelation often results in autocorrelation of the model

Table 6. R^2 from the generalized inversion setting (Gen.) compared to the maximum R^2 from all inversion settings (Max.). Using all models with significant models (sample size n), the percentile (Pct.) of the generalized model R^2 was calculated.

	Crack Porosity Measurement Depth															
	----------m----------															
	0.25				0.5				0.75				1			
Region	R^2				R^2				R^2				R^2			
Size	Max.	Gen.	Pct.	n	Max.	Gen.	Pct.	n	Max.	Gen.	Pct.	n	Max.	Gen.	Pct.	n
--m^2--	----------		-%-	---	----------		-%-	---	----------		-%-	---	----------		-%-	---
0.02	0.12	0.10	91	343	0.06	0.06	96	343	0.10	0.08	88	343	0.04	0.02	73	337
0.06	0.28	0.26	92	343	0.16	0.12	77	343	0.29	0.26	94	343	0.11	0.09	94	341
0.14	0.40	0.34	85	342	0.28	0.20	71	343	0.46	0.38	86	343	0.20	0.13	77	326
0.25	0.57	0.44	80	343	0.25	0.18	56	330	0.49	0.46	85	343	0.22	0.17	99	291
0.39	0.64	0.40	83	338	0.49	0.29	62	216	0.61	0.54	93	343	0.49	0.40	96	328
0.56	0.60	0.48	91	263	0.51	0.32	39	232	0.54	0.43	80	286	0.54	0.35	81	195
0.77	0.54	0.47	90	261	0.33	0.20	0	34	0.63	0.52	93	253	0.47	0.34	61	42
1	0.64	0.47	54	209	0.51	0.02	0	24	0.66	0.24	0	48	0.41	0.07	0	6

Table 7. RMSE from the generalized inversion setting (Gen.) compared to the minimum RMSE from all inversion settings (Min.). Using all models with significant models (sample size n), the percentile (Pct.) of the generalized model R^2 was calculated.

	Crack Porosity Measurement Depth															
	----------m----------															
	0.25				0.5				0.75				1			
Region	RMSE				RMSE				RMSE				RMSE			
Size	Min	Gen.	Pct.	n	Min	Gen.	Pct.	n	Min	Gen.	Pct.	n	Min	Gen.	Pct.	n
--m^2--	----m^3m^{-3}----		-%-	---	----m^3m^{-3}----		-%-	---	----m^3m^{-3}----		-%-	---	----m^3m^{-3}----		-%-	---
0.02	0.098	0.099	91	343	0.075	0.075	96	343	0.090	0.091	88	343	0.084	0.085	73	337
0.06	0.062	0.063	93	343	0.046	0.046	77	343	0.050	0.051	94	343	0.053	0.054	95	341
0.14	0.041	0.044	86	342	0.032	0.033	70	343	0.032	0.034	87	343	0.039	0.041	77	326
0.25	0.034	0.039	80	343	0.028	0.029	56	330	0.025	0.025	85	343	0.032	0.033	99	291
0.39	0.026	0.034	83	338	0.019	0.023	61	216	0.020	0.022	94	343	0.026	0.028	97	328
0.56	0.023	0.026	91	263	0.016	0.018	38	232	0.016	0.018	80	286	0.021	0.025	80	195
0.77	0.018	0.019	90	261	0.019	0.020	-	34	0.013	0.015	93	253	0.024	0.026	60	42
1	0.015	0.018	53	209	0.013	0.018	-	24	0.009	0.013	-	48	0.017	0.022	-	6

residuals which violates one of the primary assumptions of ordinary least squares regression. Using the Moran's I, the residuals of models with region size above 0.25m^2, spatial autocorrelation of residuals could not be detected.

Although the generalized models performed well, they never had the highest R^2 or lowest RMSE. While other models resulted in lower RMSE and higher R^2, it is unclear if these models were significantly different from the generalized inversion setting. To test for statistical diffrences we will focus on data from only 0.56 m^2 region size. We selected this region size because at this scale, model residuals were uncorrelateshowed no spatial autocorrelationd. Additionnally, at this scale the generalized inversion model preformend poorest averaging in the 72nd percentile across all depths. If a signifianct diffrence exhisted between the best preformeing model and the generalized model, it will be most apparent when the generalized model is preforming most poorley. To facillitate comparsions of models from inversions with different MR parameter vlaues, we normalized electrical resistivity data by maximum electrical resistivity. This resulted in data scaled between zero and one. Analysis of covariance showed that, for each crack porosity measurement depth, the slope terms of the generalized inversion model and the maximum models were not significantly different at the 95% confidence level (Table 8). Despite the fact that the maximum models resulted in a higher R^2 and lower RMSE, model parameters were not significantly different from the generalized model.

Table 8. Fitted linear model parameters. All model parameters were significant at the 0.99 confidence level

Crack Porosity Depth	Maximum Inversions				General Inversion			
	Intercept	Slope	R^2	RMSE	Intercept	Slope	R^2	RMSE
---m---	--------m^3m^{-3}---------		----	m^3m^{-3}	--------m^3m^{-3}---------		----	m^3m^{-3}
0.25	0.027a*	0.28a	0.60	0.023	NS	0.21a	0.48	0.026
0.5	NS**	0.15b	0.51	0.016	NS	0.10a	0.32	0.018
0.75	0.029a	0.11b	0.54	0.016	NS	0.13a	0.43	0.018
1	NS	0.17a	0.54	0.021	NS	0.16a	0.35	0.025

*Parameters in the same column followed by the same letter were not significantly different at the 0.95 level

**Parameters were not significant at the 95% confidence level

One concern with using ERT to estimate crack porosity, is that ERT may be sensitive to factors other than crack porosity such as soil water content or total shrinkage porosity. In the previous chapter, it was shown that ERT is not sensitive to soil water content when the soil is cracked. Using total shrinkage porosity calculated from soil water loss, we interpolated shrinkage porosity onto the same 0.125-m spaced grid as electrical resistivity and crack porosity data. When the interpolated crack porosity data was averaged on a region size of 0.56-m^2 regions, shrinkage porosity showed no significant correlation to electrical resistivity data (Fig. 13). This suggests that the total shrinkage porosity does not contribute to increases in bulk soil electrical resistivity.

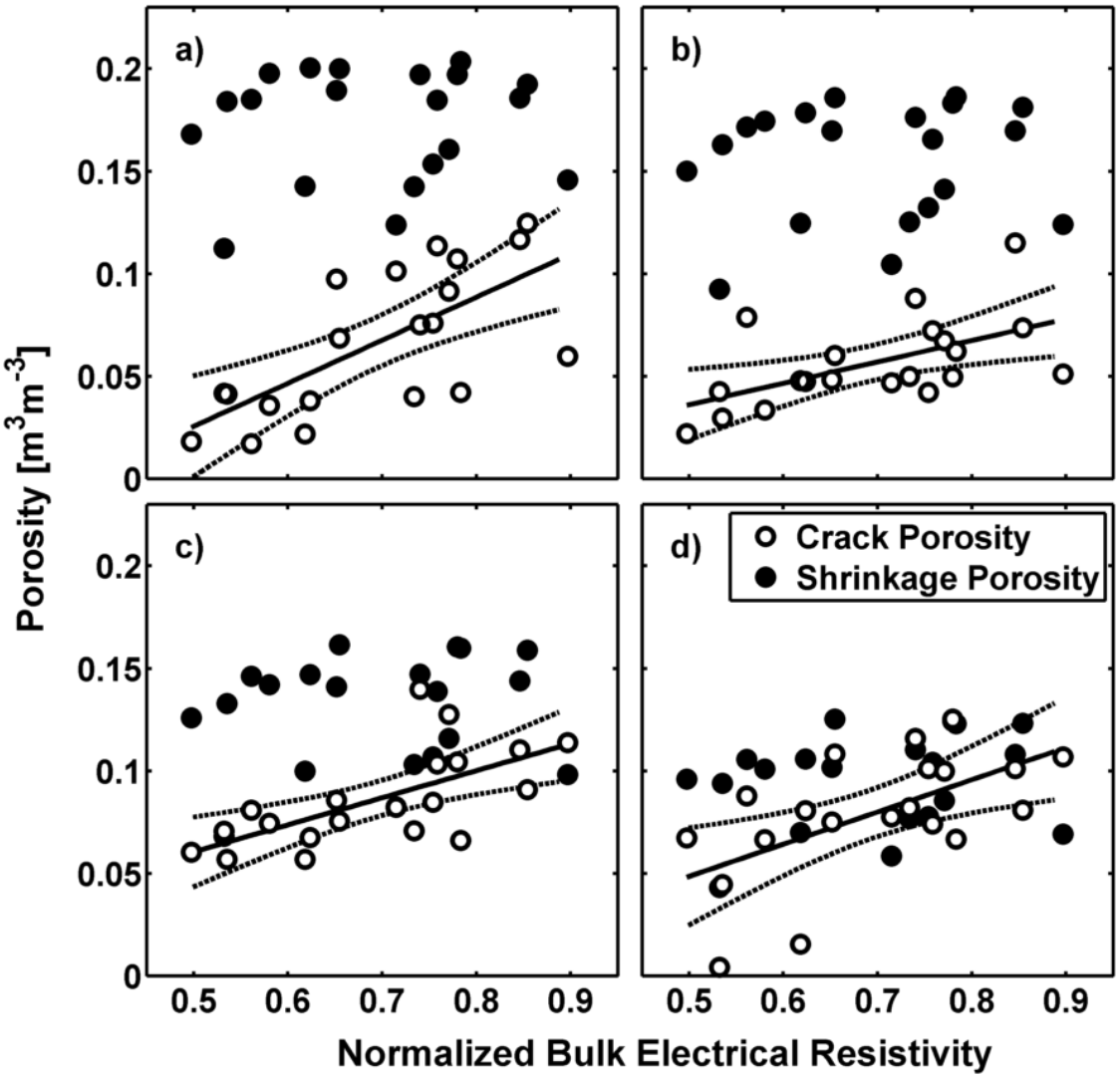

Figure 13. Final models for the generalized inversion setting. Sub-figures a, b, and c correspond to models for image depth of 0.25, 0.5, 0.75, and 1 m respectively. Dashed lines show the 95% confidence intervals of model parameters.

Conclusion

ERT has been applied in soil science for a variety of applications including estimating soil water content and solute concentration (Samouëlian et al., 2005). In the soil science literature, the role of inversion parameters in the interpretation of ERT images and data is often ignored. The results shown here demonstrate that the quality of

models based on ERT data is sensitive to inversion parameters. Future applications of ERT in soil science may benefit from a more robust investigation into the role of inversion parameters in model quality.

As a tool for measuring crack porosity, ERT has limited applicability. The models presented here proved to be poor to fair estimators of crack porosity. For crack porosity measured between 0.25 and 1 m, the generalized models had an average RMSE of 0.022 m^3m^{-3}. With crack porosity of approximately 0.05 m^3m^{-3}, model RMSE is a significant proportion of total crack porosity making estimates using such models unreliable. Additionally models developed here have limited applicability. These models calibrated and optimized for one soil using specific inversion software. If the same survey design and inversion settings were used on other soils, there is no guarantee that these models would accurately predict crack porosity. With other survey designs that utilize more electrodes or electrodes installed in the subsurface, it may be possible to improve the quality of observed relationships between bulk electrical resistivity and crack porosity. However, such improvements would require a significant investment of resources with no guarantee of improved performance.

CHAPTER IV

CONCLUSIONS

Soil electrical resistivity and water content were measured concurrently under laboratory conditions and in the field. Laboratory measurements made on intact soil cores and in the absence of cracks showed that the relationship between soil matrix electrical resistivity and water content could be modeled using a well defined power relationship. Under non-cracked conditions, bulk soil electrical resistivity from field ERT surveys agreed well with predictions of matrix electrical resistivity made using the laboratory calibration model. When cracks were present, bulk electrical resistivity showed a significant positive bias compared to predictions of matrix electrical resistivity with the magnitude of bias decreasing with depth. When crack were present, bulk electrical resistivity could not be used to predict soil water content. These results support the conclusion that ERT is strongly influenced by the presence of cracks.

Total shrinkage-generated porosity was estimated form measurement of soil water content. When compared to measurements of crack porosity, results showed that up to a depth of 1-m, total shrinkage generated porosity exceeded crack porosity. This suggests that only a portion of total shrinkage volume is partitioned into vertical cracks with the remaining portion contributing to horizontal cracks or inter-aggregate porosity. Understanding the partitioning of total soil shrinkage into various porosity sizes classes is critical to understanding and modeling vertisol hydrology.

Increases in crack porosity were positively correlated to increases in bulk electrical resistivity. The relationship between bulk soil electrical resistivity and crack porosity could be modeled using a simple linear model. Changes in ERT inversion settings resulted in changes in the accuracy and quality of fit of these linear models. Depending on the inversion setting, for the same crack porosity depth, the R^2 of linear models ranged between 0.48 and 0.60 with model RMSE ranging from 0.23 to 0.26 m^3m^{-3}. Although inversion settings affected the fit quality of linear models, no significant difference in model parameters was detected. This suggests that there is one model that can be used to relate bulk electrical resistivity across a range of inversion parameters. The poor fit of all models suggested that ERT has limited applicability for measuring crack porosity. Model prediction error was high, averaging 0.021 m^3m^{-3}. This is a significant amount of error considering that over the same depths, crack porosity averaged to 0.07 m^3m^{-3}.

Further refinements to the methodology used in this study may yield more accurate models for estimating crack porosity. However, due to the inherently inaccurate nature of ERT, the development of models that yield highly accurate crack measurements in unlikely. The results of this study suggest that the best use of ERT for monitoring cracking is to use ERT as a qualitative rather than quantities tool. The integration of ERT with other proximal sensors may be useful for identifying the locations of cracks within a field. This could be done by measuring the bias between measured bulk electrical resistivity and matrix electrical resistivity estimated from soil water content. The bias between matrix and bulk electrical resistivity could then be used

to determine if the soil was cracked. Three dimensional ERT surveys may also be valuable in identifying the relative density or volume of cracking with in moderately sized plots. This could be useful in situations where information on the relative occurrence of soils is helpful but exact measurements of crack volume is not necessary.

REFERENCES

Advanced Geosciences. 2008. Instruction manual for EarthImager 3D. Version 1.5.3. Advanced Geosciences Inc., Austin, TX.

Amato, G. Bitella, R. Rossi, J.A. Gomez, S. Lovelli, and J.J.F. Gomez. 2009. Multi-electrode 3D resistivity imaging of alfalfa root zone. Eur. J. Agron. 31:213-222.

Amidu, S.A., and J.A. Dunbar. 2007. Geoelectric studies of seasonal wetting and drying of a Texas Vertisol. Vadose Zone J. 6:511-523

Archie, G.E. 1942. The electrical resistivity log as an aid in determining some reservoir characteristics. Trans. Am. Ints. Min. Metall. Pet. Eng. 146:54-62.

Arnold, J.G., K.N. Potter, K.W. King, and P.M. Allen. 2005. Estimation of soil cracking and the effect on surface runoff in a Texas Blackland Prairie watershed. Hydrol. Process 19:589-603.

Baer, J.U., T.F. Kent, and S.H. Anderson. 2009. Image analysis and fractal geometry to characterize soil desiccation cracks. Geoderma. 154:153-163.

Bouma, J. 1981. Soil morphology and preferential flow along macropores. Agric. Water. Manage. 3:235-250.

Bovin, P., 2007. Anisotropy, cracking, and shrinkage of Vertisol samples - experimental study and shrinkage modeling. Geoderma. 138:25-37.

Bronswijk, J.J.B. 1989. Prediction of actual cracking and subsidence in clay soils. Soil Sci.148:87-93.

Brunet, P., R. Clement, and C. Bouvier. 2010. Monitoring soil water content and deficit

using electrical resistivity tomography (ERT) - a case study in the Cevennes area, France. J. Hydrol. (Amsterdam). 380:146-153.

Campbell, G.S., and J.M. Norman. 1998. An introduction to environmental biophysics. 2nd ed. Springer Sci. Business Media, New York.

Cassiani, G., A. Gordio, S. Stocco, A. Villa, R. Deiana, P. Frattini, and M. Rossi. 2009. Monitoring the hydrologic behaviour of a mountain slope via time-lapse electrical resistivity tomography. Near Surf. Geophys. 7:475-486.

Chansyk, D.S., and M.A. Naeth. 1996. Field measurement of soil moisture using neutron probes. Can. J. Soil Sci. 76:317-323

Cheng, Y., and D.E. Pettry. 1993. Horizontal and vertical movements of 2 expansive soils in Mississippi. Soil Sci. Soc. Am. J. 57:1542-1547.

Constable, S.C., R.L. Parker, and C.G. Constable, 1987. Occam's inversion:a practical algorithm for generating smooth models from electromagnetic sounding data. Geophys. 52:298-300.

Coquet, Y. 1998. In situ measurement of the vertical linear shrinkage curve of soils. Soil Tillage Res. 46:289-299.

Daily, W., A. Ramirez, D. Labreque, and J. Nitao. 1992. Electrical-resistivity tomography of vadose water-movement. Water Resour. Res. 28:1429-1442.

Dasog, G.S., and G.B. Shashidhara. 1993. Dimension and volume of cracks in a vertisol under different crop covers. Soil Sci. 6:424-428.

Dey, A., and H.F. Morrison. 1979. Resistivity modiling for arbitrarily shaped two-dimensional structures. Geophys. Prosp. 27:106-136.

Dinka, T.M., C.L.S. Morgan, K.J. McInnes, A.S. Kishne, and R.D. Harmel. 2013. Shrink-swell behavior of soil across a Vertisol catena. J. Hydrol. 476:352-359.

El Abedine Z., A., and G.H. Robinson. 1971. Study on cracking in some Vertisols of Sudan. Geoderma. 5:229-241

Fityus, S., T. Wells, and H. Wenxiong. 2011. Water content measurement in expansive clay soils using neutron probe. Geotech. Test. J. 34:255-264.

French, H., and A. Binely. 2004. Snowmelt infiltration: monitoring temporal and spatial variability using time-lapse electrical resistivity. J. Hydrol. (Amsterdam). 297:174-186

Frohlich, R.K., and C.D. Park. 1989. The electrical-resistivity of the vadose zone - field survey. Ground Water. 27:524-530.

Garré, S., J. Koestel, T. Gunther, M. Javaux, J. Vanderborght, and H. Vereecken. 2010. Comparison of heterogeneous transport processes observed with electrical resistivity tomography in two soils. Vadose Zone J. 9:336-349.

Garré, S., M. Javaux, J. Vanderborght, L. Pages, and H. Vereecken. 2011. Three-dimensional electrical resistivity tomography to monitor root zone water dynamics. Vadose Zone J. 10:412-424.

Gee, G.W., and J.W. Bauder. 1986. Particle-size analysis. In: A. Klute, editor, Methods of soil analysis. Part 1. 2nd ed. Agron. Monogr. 9. ASA and SSSA, Madison, WI. p. 383-411.

Glover, P.W.J., M.J. Hole, and J. Pous. 2000. A modified Archie's law for two conducting phases. Earth Planetary Sci. Lett. 180:369-383.

Greve, A.K., R.I. Acworth, and B.F.J. Kelly. 2010. Detection of subsurface soil cracks by vertical anisotropy profiles of apparent electrical resistivity. Geophys. 75(4):85-93.

Greve, A., M.S. Andersen, R.I. Acworth. 2010. Investigations of soil cracking and preferential flow in a weighing lysimeter filled with cracking clay soil. J. Hydrol. (Amsterdam). 393:105-113.

Keller, G.V., and F.C. Frischknecht. 1966. Electrical methods in geophysical prospecting. Pergamon Press, Oxford, UK.

Kirby, J.M., A.L. Bernardi, A.J. Ringrose-Voase, R. Young, and H. Rose. 2003. Field swelling, shrinking, and water content change in a heavy clay soil. Aust. J. Soil Res. 41:963-978.

Kishné, A.Sz., C.L.S. Morgan, and W.L. Miller. 2009. Vertisol crack extent associated with gilgai and soil moisture in the Texas Gulf Coast prairie. Soil Sci. Soc. Am. J. 73:1221-1230.

Lakshmikantha, M.R., P.C. Prat, and A. Ledesma. 2009. Image analysis for the quantification of a developing crack network on a drying soil. Geotech. Test. J. 32:505-515.

Lesch, S.M., and D.L. Corwin. 2003. Using the dual-pathway parallel conductance model to determine how different soil properties influence conductivity survey data. Agron. J. 95:365-379.

MathWorks. 2012. Image processing toolbox: Color-based segmentation using k-means clustering (R2012a). MathWorks Inc., Natick, MA.

Michot, D., Y. Benderitter, A. Dorigny, B. Nicoulliad, D. King, and A. Tabbagh. 2003. Spatial and temporal monitoring of soil water content with an irrigated corn crop cover using surface electrical resistivity tomography. Water. Resour. Res. 39:1138-1158.

Oldenburg, D. 1990. Inversion of electromagnetic data - an overview of new techniques. Surv. Geophys. 11:231-270.

Olsen, P.A., and L.E. Haugen. 1998. New model of the shrinkage characteristic applied to some Norwegian soils. Geoderma 83:67-81.

Panissod, C., M. Dabas, A. Jolivet, and A. Tabbagh. 1997. A novel mobile multipole system (MUCEP) for shallow (0-3m) geoelectrical investigation: the 'Vol-de-canards' array. Geophys. Prosp. 45:983-1002.

Pellerin, L., 2002. Applications of electrical and electromagnetic methods for environmental and geotechnical investigations. Surv. Geophys. 23:101-132.

Peng, X., R. Horn, S. Peth, and A. Smucker. 2006. Quantification of soil shrinkage in 2D by digital image processing of soil surface. Soil Tillage Res. 91:173-180.

R Core Team. 2013. R: A language and environment for statistical computing. R Foundation for Statistical Computing, Vienna, Austria.

Rey, E., D. Jongmans, P. Gotteland, and S. Garambois. 2006. Characterisation of soils with stony inclusions using geoelectrical measurements. J. Appl. Geophys. 2005. 188-201.

Rhoades, J.D., P.A.C. Raats, and R.J. Prather. 1976. Effects of liquid-phase electrical-conductivity, water-content, and surface conductivity on bulk soil electrical-

conductivity. Soil Sci. Am. J. 40:651-655.

Ringrose-Voase, A.J., and W.B. Sanidad. 1996. A method for measuring the development of surface cracks in soils: Application to crack development after lowland rice. Geoderma. 71:245-261.

Rings, J., A. Scheuermann, K. Perko, and C. Hauck. 2008. Soil water content monitoring on a dike model using electrical resistivity tomography. Near Surf. Geophys. 6:123-132.

Ritchie, J.T., and J.T. Adams. 1974. Field measurement of evaporation from soil shrinkage cracks. Soil Sci. Soc. Am. J. 38:131-134.

Robinson, E.S., and C. Coruh. 1988. Basic exploration geophysics. John Wiley & Sons, New York.

Samouëlian, A., I. Cousin, G. Richard, A. Tabbagh, and A. Bruand. 2003. Electrical resistivity imaging for detecting soil cracking at the centimetric scale. Soil Sci. Am. J. 67:1319-1326.

Samouëlian, A., G. Richard, I. Cousin, R. Guerin, A. Braund, and A. Tabbagh. 2004. Three-dimensional crack monitoring by electrical resistivity measurement. Eur. J. Soil Sci. 55:751-762.

Samouëlian, A., I. Cousin, A. Tabbagh, A. Braund, and G. Richard. 2005. Electrical resistivity survey in soil science: a review. Soil Tillage Res. 83:173-193.

Schwartz, B.F., M.E. Schreiber, and T.T. Yan. 2008. Quantifying field-scale soil moisture using electrical resistivity imaging. J. Hydrol. (Amsterdam). 362:234-246.

Seladji, S., P. Cosenza, A. Tabbagh, J. Ranger, and G. Richard. 2010. The effect of compaction on soil electrical resistivity: a laboratory investigation. Eur. J. Soil Sci. 61:1043-1055.

Sentenac, P. and M. Zielinski. 2009. Clay fine fissuring monitoring using miniature geo-electrical resistivity arrays. Environ. Earth Sci. 59:205-214.

Sharma, R.B., and G.P. Verma. 1977. Characterization of shrinkage cracks in medium black clay soil of Madhya-Pradesh: I Pattern and size of cracking in relation to vegetative covers. Plant Soil. 48:323-333.

Sherrod, L.A., G. Dunn, G.A. Peterson, and R.L. Kolberg. 2002. Inorganic carbon analysis by modified pressure-calcimeter method. Soil Sci. Am. J. 66:299-305.

Soil Survey Staff. 1996. Soil survey laboratory methods manual. Soil Survey Investigations. Report No.42. U. S. Govt. Printing Office, Washington, D. C.

Soil Survey Staff. 2012. Web Soil Survey. http://websoilsurvey.nrcs.usda.gov/ (accessed October 15, 2012).

Srayeddin, I., and C. Doussan. 2009. Estimation of the spatial variability of root water uptake of maize and sorghum at the field scale by electrical resistivity tomography. Plant Soil. 319:185-207.

Tetagan, M., C. Pasquier, A. Besson, B. Nicoullaud, A. Bouthier, H. Bourennane, C. Desbourdes, D. King, and I. Cousin. 2012. Field-scale estimation of the volume percentage of rock fragments in stony soils by electrical resistivity. Catena. 92:67-74.

Velde, B., 1999. Structure of surface cracks in soil and muds. Geoderma. 93:101-124.

Velde, B. 2001. Surface cracking and aggregate formation observed in a Rendzina soil, La Touche (Vienne) France. Geoderma. 99:261-276.

Vogel, H.J., U. Weller, and U. Babel. 1993. Estimating orientation and width of channels and cracks at soil polished blocks - a stereological approach. Geoderma. 56:301-316.

Vogel, H.J., H. Hoffman, and K. Roth. 2005. Studies of crack dynamics in clay soil - I. Experimental methods, results, and morphological quantification. Geoderma. 125:203-211.

Waller, P.M., and W.W. Wallender, 1993. Changes in cracking, water-content, and bulk-density of salinized swelling clay field soils. Soil Sci. 156:414-423.

Waxman, H.M., and L.J. Smits. 1968. Electrical conductivities in oil-bearing shaly sands. Soc. Petrol. Eng. J. 8:107.

Yassoglou, N., C.S. Kosmas, N. Moustakas, E. Tzianis, and N.G. Danalatos. 1994. Cracking in recent alluvial soils as related to easily determined soil properties. Geoderma. 63:289-298.

Zhang, J., R.L. Mackie, and T.R. Madden. 1995. 3-D resistivity forward modeling and inversion using conjugate gradients. Geophys. 60:1313-1325.

Zhou, B., and T. Dahlin. 2003. Properties and effects of measurement errors on 2D resistivity imaging surveying. Near Surf. Geophys. 1:105-117.

Zhou, Q.Y., J. Shimada, and A. Sato. 2001. Three-dimensional spatial and temporal monitoring of soil water content using electrical resistivity tomography. Water Resour. Res. 37:273-285.